Article

Dominant Driving Forces in Human Telomere Quadruplex Binding-Induced Structural Alterations

Matjaž Bončina,[1] Florian Hamon,[2] Barira Islam,[3] Marie-Paule Teulade-Fichou,[2] Gorazd Vesnaver,[1] Shozeb Haider,[3,4] and Jurij Lah[1,*]

[1]Faculty of Chemistry and Chemical Technology, University of Ljubljana, Ljubljana, Slovenia; [2]Institut Curie, Centre National de la Recherche Scientifique UMR-176, Centre Universitaire d'Orsay, Orsay, France; [3]Centre for Cancer Research and Cell Biology, Queen's University of Belfast, Belfast, UK; and [4]University College London School of Pharmacy, Bloomsbury, London, UK

ABSTRACT Recently various pathways of human telomere (ht) DNA folding into G-quadruplexes and of ligand binding to these structures have been proposed. However, the key issue as to the nature of forces driving the folding and recognition processes remains unanswered. In this study, structural changes of 22-mer ht-DNA fragment (Tel22), induced by binding of ions (K^+, Na^+) and specific bisquinolinium ligands, were monitored by calorimetric and spectroscopic methods and by gel electrophoresis. Using the global model analysis of a wide variety of experimental data, we were able to characterize the thermodynamic forces that govern the formation of stable Tel22 G-quadruplexes, folding intermediates, and ligand-quadruplex complexes, and then predict Tel22 behavior in aqueous solutions as a function of temperature, salt concentration, and ligand concentration. On the basis of the above, we believe that our work sets the framework for better understanding the heterogeneity of ht-DNA folding and binding pathways, and its structural polymorphism.

INTRODUCTION

Guanine-rich DNA sequences in the presence of cations can fold into four-stranded structures called G-quadruplexes. The existence of potential quadruplex sequences in key regions of the eukaryotic genome, including the immunoglobulin heavy chain switch region, promoter regions, ribosomal DNA, oncogenes, and telomeres, suggests that they may play an important role in the mechanism and control of several cellular processes (1–3). Therefore, G-quadruplexes are relevant targets of small molecules that can potentially modulate their biological functions, gene expression, and protein synthesis (4,5).

Quadruplex topologies may differ in glycosidic bond angles, strand orientation, connecting loop regions, and molecularity leading to conformational heterogeneity of G-quadruplex structures. This is well exemplified by guanine-rich human telomeric (ht) repeat sequences, which are capable of adopting multiple topologies. For example, monomeric ht quadruplexes containing the core sequence $d(AGGG(TTAGGG)_3)$ (Tel22) can adopt several distinct quadruplex topologies. X-ray crystallography reveals that in the presence of K^+ ions, Tel22 shows all-parallel strand orientation (6) while in K^+ solutions it adopts, according to NMR and other biophysical techniques, a (3+1) hybrid-type topology (denoted as H_{K^+}) (7–10). By contrast, in Na^+ solutions Tel22 adopts a conformation with antiparallel strand orientation (denoted as A_{Na^+}) (11). As shown recently, binding of ligands capable of inducing binding-coupled conformational transitions of G-quadruplexes may be an additional cause of the observed ht-quadruplex polymorphism (12–16).

Detailed computational and experimental (thermodynamic, kinetic) investigation of folding and ligand binding pathways of quadruplex DNA has begun very recently (17–22). These studies leave no doubt that in solution, the Tel22 folding/unfolding process may consist of several structural steps, meaning that such solutions should be considered as equilibrium mixtures of Tel22 molecules in their folded (Q), unfolded (U), and intermediate (I) states. Because in the reported studies of ligand binding to Tel22, as a rule, the involvement of Tel22 folding intermediates has been neglected, one may expect the reported thermodynamics of binding to be incomplete. Thus, in addition to investigating the nature and the relative importance of forces that govern folding of Tel22 and its recognition by ligands, we aimed to estimate how important in controlling these binding events may be the involvement of the Tel22 intermediates. We believe that such an approach will lead to an improvement in our understanding of the heterogeneity observed in the ht-quadruplex folding and binding processes, and of the complex interplay between the enthalpic and entropic contributions to the free energy changes accompanying these events.

MATERIALS AND METHODS

Sample preparation

HPLC pure oligonucleotide 5′-AGGGTTAGGGTTAGGGTTAGGG-3′ (Tel22) was obtained from Midland Chemical (Midland, MI). The buffer

Submitted January 9, 2015, and accepted for publication May 3, 2015.

*Correspondence: jurij.lah@fkkt.uni-lj.si

Editor: Timothy Lohman.

0006-3495/15/06/2903/9 $2.00

http://dx.doi.org/10.1016/j.bpj.2015.05.001

solutions used in our experiments consisted of 20 mM cacodylic acid, 1 mM EDTA, and various concentrations of Na^+ or K^+ ions. NaOH (KOH) was added to cacodylic acid to reach pH = 6.9. Then, NaCl (KCl) was added to obtain the desired concentration of Na^+ (K^+) ions (100 or 200 mM Na^+ (K^+) in cacodylic buffer). DNA was first dissolved in water and then extensively dialyzed against the buffer using a Float-A-Lyser dialysis tube (molecular mass cutoff 500–1000 Da; Spectrum Laboratories, Piscataway, NJ). The starting solution of oligonucleotide was first heated up to 95°C in an outer thermostat for 5 min to make sure that all DNA transforms into the unfolded form, and subsequently cooled down to 5°C at the cooling rate of 0.05°C min^{-1} to allow DNA to adopt quadruplex structure(s). It is then used in the experiments. Concentration of the DNA in the buffer solution was determined at 25°C spectrophotometrically using a Cary 100 BIO UV/Visible Spectrophotometer (Varian, Cary, NC) equipped with a thermoelectric temperature controller. Tel22 concentrations at 25°C were obtained from the melting curves monitored at wavelength $\lambda = 260$ nm. For the extinction coefficient of Tel22 unfolded form at 25°C, we used the value $\varepsilon_{260} = 228{,}500\ M^{-1}\ cm^{-1}$ estimated from the nearest-neighbor data of Cantor et al. (23).

The two bisquinolinium derivatives, Phen-DC3 (M = 848.12 g mol^{-1}; Fig. S1 in the Supporting Material), and 360A-Br (M = 780.90 g mol^{-1}; Fig. S1), are poorly soluble in aqueous solution, therefore they were first dissolved in DMSO and then transferred into buffer solution. The lowest possible content of the DMSO in the buffer solution sufficient for ligand solubility (μM range) was 3%. Therefore, all quantities of the ligand and Tel22 were dissolved in buffer solution with 3% DMSO. Concentrations of the ligands were determined by measuring absorbance at 25°C ($\varepsilon_{\text{Phen-DC3, 350 nm}} = 6200\ M^{-1}\ cm^{-1}$ and $\varepsilon_{\text{360A-Br, 370 nm}} = 5980\ M^{-1}\ cm^{-1}$).

Circular dichroism spectroscopy

Circular dichroism (CD) spectra of DNA and ligand-DNA complexes were recorded at 25°C in a 1.0 cm cuvette in the wavelength range between 215 and 350 nm. CD titrations were conducted at 25°C by titrating DNA solution ($c_{\text{DNA}} \approx 70\ \mu$M) into a 600 μL ligand solution ($c_L \approx 20\ \mu$M). Ellipticity, Θ, was measured at 293 nm in a 1.0 cm cuvette with signal averaging time of 30 s and 5 nm bandwidth. Temperature dependence of CD spectra of Tel22 was collected between 215 and 320 nm in a 0.25 mm cuvette with a signal averaging time of 10 s and 5 nm bandwidth. Experiments were performed using a CD spectrophotometer model No. 62A DS (Aviv Biomedical, Lakewood, NJ) equipped with a thermoelectric temperature controller.

Fluorimetry

Fluorimetry (FL) titrations were conducted at 25°C by titrating DNA solution ($c_{\text{DNA}} \approx 80\ \mu$M) into a 1000 μL 360A-Br ligand solution ($c_L \approx 10\ \mu$M). Emission spectra were recorded between 340 and 570 nm (excitation wavelength $\lambda_{\text{ex}} = 330$ nm) in a 1.0 cm cuvette with scanning speed of 50 nm min^{-1}. Phen-DC3 exhibits very weak induced fluorescence, therefore we were unable to obtain reliable experimental data for further model analysis of its binding. Experiments were performed using a Cat. No. LS 55 luminescence spectrometer (Perkin Elmer, Waltham, MA) equipped with a thermally controlled cell holder.

Isothermal titration calorimetry

Isothermal titration calorimetry (ITC) experiments were performed between 15 and 35°C by titrating a solution of DNA ($c_{\text{DNA}} \approx 80\ \mu$M) into a ligand solution ($c_L \approx 10\ \mu$M, $V = 1.386$ mL) using a VP-ITC isothermal titration calorimeter from Microcal (Northampton, MA). The area under the peak after each injection of DNA solution was obtained by integration of the raw signal, corrected for the corresponding heat of dilution (blank titration of DNA into buffer solution) and expressed per mole of added DNA per injection, to give the enthalpy of interaction, (ΔH_T).

Differential scanning calorimetry

Differential scanning calorimetry (DSC) experiments were performed at the DNA concentration of ~0.3 mM in the temperature range between 1 and 95°C at the heating and cooling rate of 1.0°C min^{-1}. The corresponding baseline (buffer-buffer) thermograms were subtracted from the heating thermograms and the obtained differences were normalized to 1 mol of DNA to obtain the partial molar heat capacity of DNA as a function of temperature. Data were analyzed in the same way as described in Bončina et al. (24). DSC experiments were performed using the Nano DSC instrument (TA Instruments, New Castle, DE).

RESULTS AND DISCUSSION

Thermodynamic analysis of binding-induced structural transitions

We investigated thermodynamics of Tel22 structural transitions in solution at various temperatures, concentrations of K^+ or Na^+ ions, and in the presence or absence of bisquinolinium ligands Phen-DC3 and 360A-Br (Fig. S1); these ligands are known for their high affinity for G-quartets, most likely due to strong π-π stacking interactions (25–28). The analysis of calorimetric (DSC and ITC) and spectroscopic (CD and FL) data obtained in solutions with K^+ (see Fig. 2; Figs. S4 and S6) or Na^+ ions (Figs. S3, S5, and S7) suggests that the observed unfolding and binding processes may be described by the model mechanism that involves five macroscopic states (Fig. 1). Reversibility of folding/unfolding of Tel22 in the absence of ligands and in the presence of K^+ or Na^+ ions ($U \leftrightarrow I \leftrightarrow Q$; Fig. S3) was verified by DSC while the reversibility of ligand binding ($Q + L \leftrightarrow Q'L + L \leftrightarrow Q''L_2$) was verified by gel electrophoresis (Fig. S11). For a given model mechanism (Fig. 1), one can write a general equation for the spectroscopic and calorimetric properties of the ligand-DNA solution, measured in the presence of K^+ or Na^+ ions (Eq. 1), from which the corresponding contributions of the buffer are subtracted. Such property, X, can be presented as a linear combination of molar ratios, $\alpha_j = c_j/c_{\text{DNA}}$ of all species, j, predicted by the model mechanism ($j = L$, U, I, Q, $Q'L$, and $Q''L_2$),

$$X = X_L\alpha_L + X_U\alpha_U + X_I\alpha_I + X_Q\alpha_Q + X_{Q'L}\alpha_{Q'L} + X_{Q''L_2}\alpha_{Q''L_2}. \quad (1)$$

In Eq. 1, X_j represents the property of the solute j at a given pressure, and it includes the temperature T, the salt type

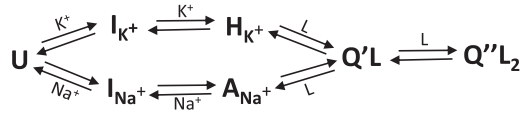

FIGURE 1 Mechanism of Tel22 structural transitions induced by binding of K^+ or Na^+ ions and bisquinolinium ligand (L = Phen-DC3 or 360A-Br) consistent with all experimental data.

(KCl and NaCl), the salt concentration, and the total DNA concentration c_{DNA}. Because according to the model $\alpha_U + \alpha_I + \alpha_Q + \alpha_{Q'L} + \alpha_{Q''L_2} = 1$ and $\alpha_L + \alpha_{Q'L} + 2\alpha_{Q''L_2} = r$, where $r = c_{L,tot}/c_{DNA} = n_{L,tot}/n_{DNA}$ ($c_{L,tot}$ is the total ligand concentration), one obtains

$$X = X_L r + (\Delta X_{IU} + \Delta X_{QI})\alpha_U + \Delta X_{QI}\alpha_I + X_Q + \Delta X_{Q'L}\alpha_{Q'L} + (\Delta X_{Q'L} + \Delta X_{Q''L_2})\alpha_{Q''L_2}, \quad (2)$$

where the changes $\Delta X_{IU} = X_U - X_I$, $\Delta X_{QI} = X_I - X_Q$, $\Delta X_{Q'L} = X_{Q'L} - X_Q - X_L$, and $\Delta X_{Q''L_2} = X_{Q''L_2} - X_{Q'L} - X_L$ refer to each step in the model mechanism presented in Fig. 1. From Eq. 2 are derived various model functions (see Eqs. S3–S6 and S9 in the Supporting Material) expressed in terms of a set of adjustable parameters that describe the CD ($X = [\Theta] = \Theta/(c_{DNA}l)$ = normalized ellipticity at given λ), FL ($X = [F] = I_F/(c_{DNA}l)$ = normalized emitted fluorescence measured at given λ), and DSC and ITC ($X = H$ = enthalpy of solution per mol of DNA) experiments. Each step in the suggested mechanism is described in terms of the corresponding changes of three standard thermodynamic parameters that are independent of the Na^+ or K^+ concentration. Two of them, $\Delta G^o_{i(T_0)}$ and $\Delta H^o_{i(T_0)}$, depend on temperature and are thus determined at the reference temperature $T_0 = 298.15$ K, while the third parameter, $\Delta C^o_{P,i}$, is assumed to be temperature-independent. These three parameters define the standard free energy and enthalpy of folding or binding, $\Delta G^o_{i(T)}$ and $\Delta H^o_{i(T)}$, at any value of T through the Gibbs-Helmholtz relation $[\partial(\Delta G^o_{i(T)}/T)/\partial T]_P = -\Delta H^o_{i(T)}/T^2$ and the Kirchhoff's law $[\partial \Delta H^o_{i(T)}/\partial T]_P = \Delta C^o_{P,i}$.

Each step is usually described in terms of the apparent $\Delta G^o_{i(T,X^+)}$ (note that X^+ stands for Na^+ or K^+), which depends on the salt concentration. Its relation with the true thermodynamic $\Delta G^o_{i(T)}$ is given by

$$\Delta G^o_{i(T,X^+)} = \Delta G^o_{i(T)} + \Delta n_i RT \ln[X^+] = \Delta G^o_{i(T_0)} T/T_0 + \Delta H^o_{i(T_0)}[1 - T/T_0] + \Delta C^o_{P,i}[T - T_0 - T\ln(T/T_0)] + \Delta n_i RT \ln[X^+], \quad (3)$$

where parameter Δn_i represents the number of ions released or uptaken in the transition step i and is assumed to be independent of T (29). Note that equilibrium molar concentration of unbound X^+, $[X^+]$, appearing in Eq. 3, is normalized to 1 M concentration in the reference (standard) state. Four thermodynamic parameters ($\Delta G^o_{i(T_0)}$, $\Delta H^o_{i(T_0)}$, $\Delta C^o_{P,i}$, and Δn_i for each step i in the suggested mechanism) define each equilibrium constant, $K_{i(T,X^+)} = \exp(-\Delta G^o_{i(T,X^+)}/RT)$, appearing in the proposed model presented in Fig. 1. In other words, 16 parameters specify the populations of species U, I, Q, $Q'L$, and $Q''L_2$ in the solution at any value of T, ligand, salt, and DNA concentration ($K_{i(T,X^+)} = f(\alpha_{j(T,X^+,r,c_{DNA})}$; $j = I, Q, Q'L, Q''L_2), \sum_j \alpha_{j(T,X^+,r,c_{DNA})} = 1$), and consequently also the corresponding CD, FL, ITC, and DSC model functions (right-hand side of Eqs. S3–S6 and S9). Global fitting of the model functions to the experimental CD, FL, ITC, and DSC data was based on the nonlinear Levenberg-Marquardt χ^2 regression procedure. The first step in the global fitting procedure was a semiglobal model analysis of DSC and CD folding/unfolding data of the ligand-free Tel22 ($U \leftrightarrow I \leftrightarrow Q$ equilibrium) in the presence of K^+ (Fig. 2, *a* and *b*) or Na^+ (Fig. S3) ions in which eight adjustable parameters were used (Table S4 in the Supporting Material). In the second step, these parameters were used in the description of the binding isotherms (Figs. 2, *c* and *d*, and S4–S7) as fixed values. Moreover, due to the high correlation between the adjustable parameters describing the $Q'L + L \leftrightarrow Q''L_2$ step, we were forced to reduce the number of the adjustable parameters. In this light, we assumed that the heat capacity and the number of ions released is the same for $Q + L \leftrightarrow Q'L$ and $Q'L + L \leftrightarrow Q''L_2$ step (Table S2). This assumption may be supported by the observed structural features of a number of (aromatic) ligand-quadruplex complexes in which the interacting surfaces of the first and the second aromatic ligand molecules, bound at the opposite ends of the G-quadruplex, are similar (30,31). Similar surface areas buried upon binding of the ligand in each step should result in similar changes in heat capacities, and, due to similar electrostatic interactions, the accompanying number of released ions should be approximately the same. Taken together, nine adjustable parameters were used in the fitting procedure in the case of Phen-DC3 (ITC and CD data; Table S5) and 11 in the case of 360A-Br (ITC, CD, and FL data).

In the absence of ligand, the folding/unfolding was described as a three-state process involving U, I, and Q (24). In K^+ or Na^+ solutions, I can be considered to be a mixture of so-called G-triplex conformations (I_{K^+} or I_{Na^+}) (19,32), which, according to the measured CD spectra, exhibit structural properties similar to H_{K^+} or A_{Na^+} (Fig. 3). Each stage of folding is in the presence of K^+ [$U \rightarrow I_{K^+} \rightarrow H_{K^+}$] and Na^+ [$U \rightarrow I_{Na^+} \rightarrow A_{Na^+}$], characterized by an extensive enthalpy-entropy compensation (33) (Fig. 4 and Table S1) and a large negative change in the heat capacity accompanying the first transition step [$U \rightarrow I$, $\Delta C^\circ_P \approx -400$ cal mol^{-1} K^{-1}]. These thermodynamic parameters are comparable with those reported for the thrombin binding aptamer folding/unfolding transition (34). Q is more thermodynamically stable ($\Delta G^\circ_{U \rightarrow Q}$ is lower) in solutions with K^+ than with Na^+ ions, which is a general characteristic of the G-quadruplex stability (35,36).

Binding of Phen-DC3 and 360A-Br to Tel22 is successfully described by the sequential binding model $Q + L \leftrightarrow Q'L + L \leftrightarrow Q''L_2$ (Figs. 2 and S4–S7), which assumes that Tel22 unfolded and intermediate states contain no binding sites. All the ligand binding experiments were performed at conditions at which the model analysis of Tel22 melting curves (Figs. 2 and S3) predicts the presence of the folding intermediates I. The fact that the global analysis of the measured binding data is appropriate (good quality of

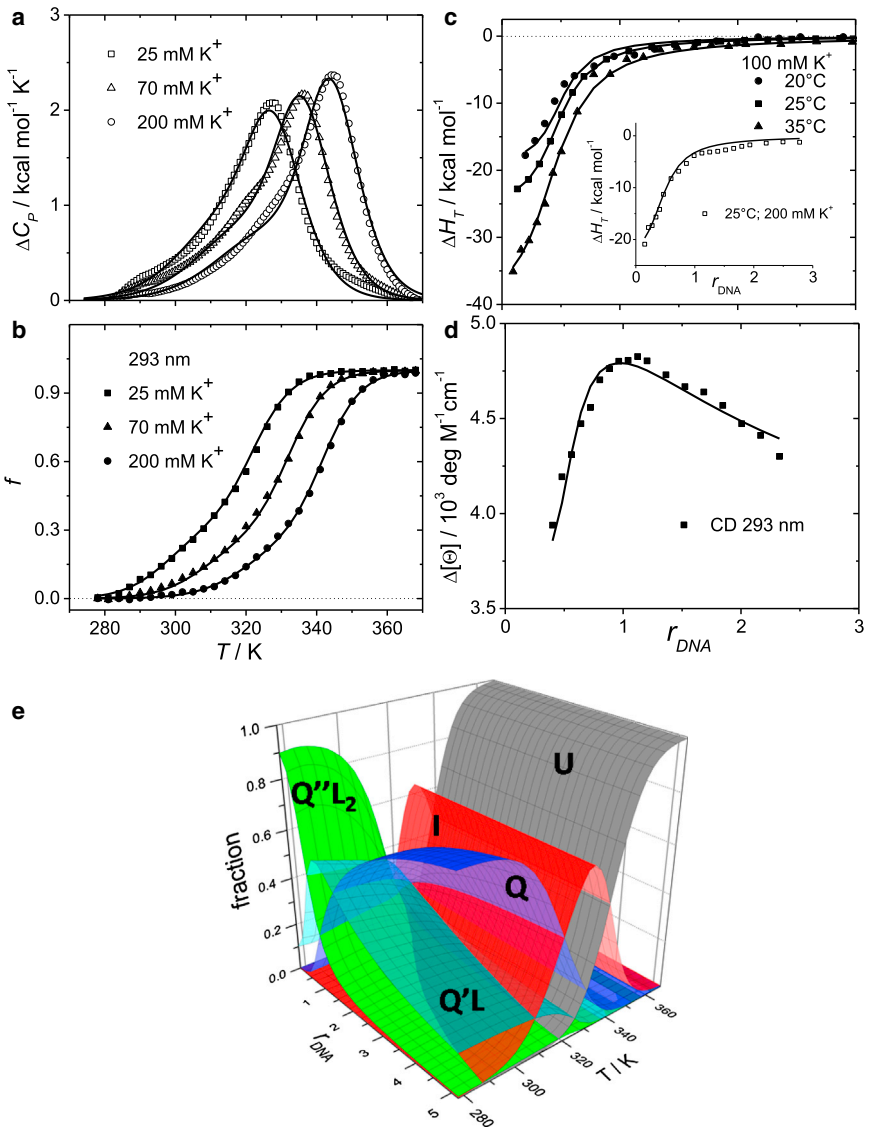

FIGURE 2 Model analysis of experimental data. Best-fit global model functions (*lines*) show good agreement with experimental data. Symbols represent unfolding data obtained by DSC and CD spectroscopy (*a* and *b*), and ligand (Phen-DC3) binding data obtained by ITC and CD spectroscopy (*c* and *d*) that is measured as a function of temperature, K^+ ion concentration, and DNA/ligand molar ratio $r_{DNA} = c_{DNA}/c_{L,tot}$ (see the Supporting Material for details). (*e*) The corresponding fractions of Tel22 species are presented as a function of the DNA/ligand molar ratio and temperature in the presence of ligand Phen-DC3 in 100 mM K^+ solution predicted by global thermodynamic analysis of data in terms of the proposed mechanism (Fig. 1). To see this figure in color, go online.

fit, reasonable values of thermodynamic parameters) only when the model-predicted population of *I* is taken into account, supports the suggested linkage between the folding and binding processes (Figs. 1, 2, *a* and *b*, and S4–S7). It should be noted that this linkage could be better supported by thermal unfolding experiments performed with ligand-DNA complexes using DSC or CD (37). Our attempts to perform such experiments and the corresponding data analysis were not successful. Namely, the detection of influence of ligand binding on melting transitions, monitored by DSC and CD spectroscopy, requires ligand concentrations that are much higher than those used in our titration experiments. In other words, due to low solubility of ligands in 100 mM K^+ or Na^+ solutions, the melting experiments cannot be performed at reversible conditions. Moreover, an adequate thermodynamic analysis of titration experiments conducted at very low K^+ or Na^+ concentrations, at which the model analysis predicts the presence of *U* and *I*, cannot be performed due to the aggregation of ligand-G-quadruplex complexes.

Taken together, Fig. 1 represents the simplest model (Model 1) of ion- and ligand-binding-induced structural alterations in the presence of K^+ and Na^+ ions, consistent with all the experimental data, whose fitting gives reliable values of thermodynamic parameters. To provide evidence that slightly simpler models are a worse fit to the data, we present in Fig. S8 some characteristics of the best global fit of the $U \leftrightarrow Q + L \leftrightarrow Q'L + L \leftrightarrow Q''L_2$ model (Model 2), which assumes that the state *I* is not populated, and the model that takes into account the $U \leftrightarrow I \leftrightarrow Q$ equilibrium and assumes that *L* binds to two equivalent independent binding sites on *Q* (Model 3). As shown in Fig. S8, Model 2 cannot describe the DSC thermograms and ITC data measured at 35°C, while Model 3 fails to describe CD titration data. On the other hand, more-complex models involve too many adjustable parameters that are highly correlated

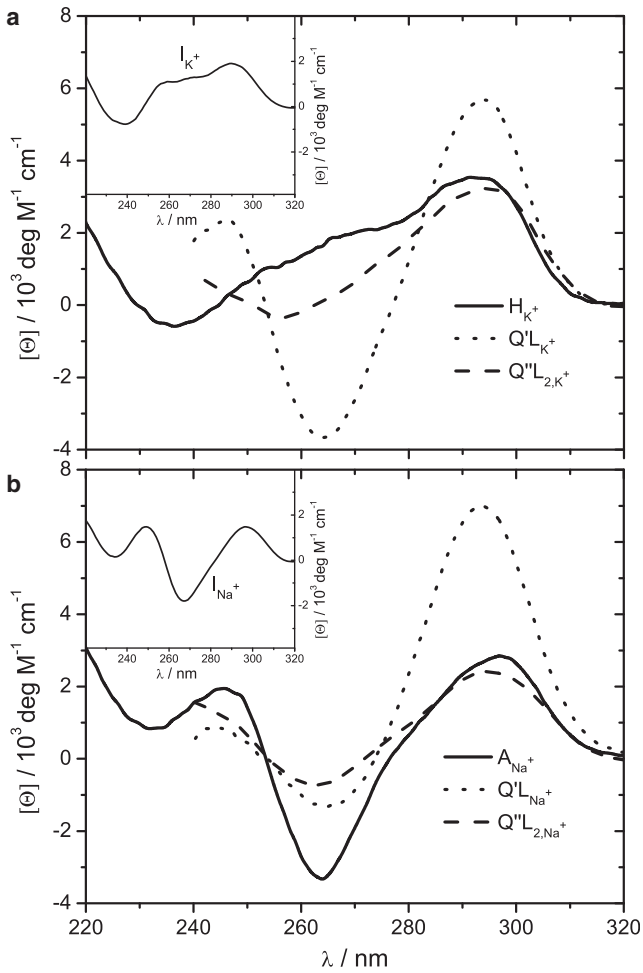

FIGURE 3 Structural features monitored by CD spectroscopy. Spectra corresponding to hybrid (H_{K^+}) and antiparallel (A_{Na^+}) structures, complexes with one ($Q'L$) and two bound ligand (L = Phen-DC3) molecules ($Q''L_2$) and folding intermediates (I_{K^+} and I_{Na^+}, see *inset*) at 25°C in the presence of 100 mM K^+ (*a*) or Na^+ (*b*) ions. CD spectra of intermediates and complexes were estimated by deconvolution of the measured spectra based on the model-predicted populations of species (Figs. S4–S7) and spectrum of Q (A_{Na^+} or H_{K^+}) form.

and thus cannot be determined with sufficient accuracy. Our analysis emphasizes an important advantage of the global fitting over the traditional fitting of the model to limited datasets (29). For example, ITC data alone (measured at $T <$ 30°C) can be successfully described by the simplified Model 3 (no I present in the solution), however, according to other available experimental data (DSC and CD titration), such analysis results in thermodynamic binding parameters that have no physical meaning.

Thermodynamics and structural features

CD spectra (Figs. 3 and S9) suggest for both ligands (Phen-DC3, 360A-Br) that their binding is accompanied by quadruplex conformational changes and that the resulting complexes ($Q'L$, $Q''L_2$) have similar structures in solutions with K^+ and Na^+ ions. CD spectra of $Q'L$ and $Q''L_2$ complexes show characteristics of the A_{Na^+} spectrum (15). Interestingly, difference CD spectra (Fig. S10) corresponding to the $Q + L \leftrightarrow Q'L$ and $Q'L + L \leftrightarrow Q''L_2$ binding events are almost mirror images, suggesting that binding of the first ligand molecule to one end of the quadruplex induces changes in CD spectrum that are opposite to those induced by binding of the second ligand molecule to the other end of the quadruplex.

The influence of the bound ligand on the conformation of the folded quadruplexes was examined also by gel electrophoresis experiments, which show that quadruplexes complexed with the ligand are electrophoretically faster than the ligand-free quadruplexes (Fig. S11). According to our model analysis, binding of dicationic ligand displaces only approximately one (nonspecifically) bound cation, which means that the net (negative) charge of the ligand-quadruplex complexes is lower than that of the ligand-free quadruplexes. Thus, if ligand binding to the quadruplex is a rigid-body association, the surface net charge of the ligand-quadruplex complex should be lower than that of the ligand-free quadruplex, and consequently the studied complexes should exhibit lower gel-mobility than the ligand-free quadruplexes (12,38). By contrast, our results (Fig. S11) show an opposite effect, i.e., an increase in mobility of the ligand-quadruplex complexes that may be, in principle, ascribed to increased hydrodynamical compactness and/or increased surface net charge of the ligand-quadruplex complexes. Because both of the two effects can arise from the increased compactness of the ligand-quadruplex complex (despite lower net, i.e., negative charge, its surface net charge can increase), we believe that the observed increased mobility of the complexes results, very likely, from the ligand-induced conformational changes of the quadruplexes. In addition, electrophoresis results suggest that, Q' and Q'' structures differ from A_{Na^+} and H_{K^+} and also from the possible all parallel Tel22 quadruplex conformation that has been shown to be gel-electrophoretically slower than A_{Na^+} and H_{K^+} (39).

The observed thermodynamic characteristics of ligand binding to Tel22 in K^+ and Na^+ solutions are very similar. For both ligands, the Q binding affinity for the first ligand molecule is higher than for the second ligand (Table S2). Both steps are enthalpy-driven, accompanied by negative change in entropy and heat capacity (Fig. 4 and Table S2). This suggests that ligand binding is driven mainly by ligand-quadruplex π-π stacking ($\Delta H^\circ < 0$) and by displacement of water from the ligand-quadruplex binding interface ($\Delta C^\circ_P < 0$). Moreover, for both ligands, the overall thermodynamics of binding-coupled folding ($U + L \rightarrow Q'L$ or $U + 2L \rightarrow Q''L_2$) is nearly the same in the K^+ and Na^+ environments (Fig. 4 and Table S2). This supports our suggestion that in solutions with either of the two ions, the ligand-bound structures are similar. In addition, $H_{K^+} + L \rightarrow Q'L_{K}{}^+$ and $A_{Na^+} + L \rightarrow Q'L_{Na}+$ (and $H_{K^+} + 2L \rightarrow Q''L_{2,K}{}^+$ and

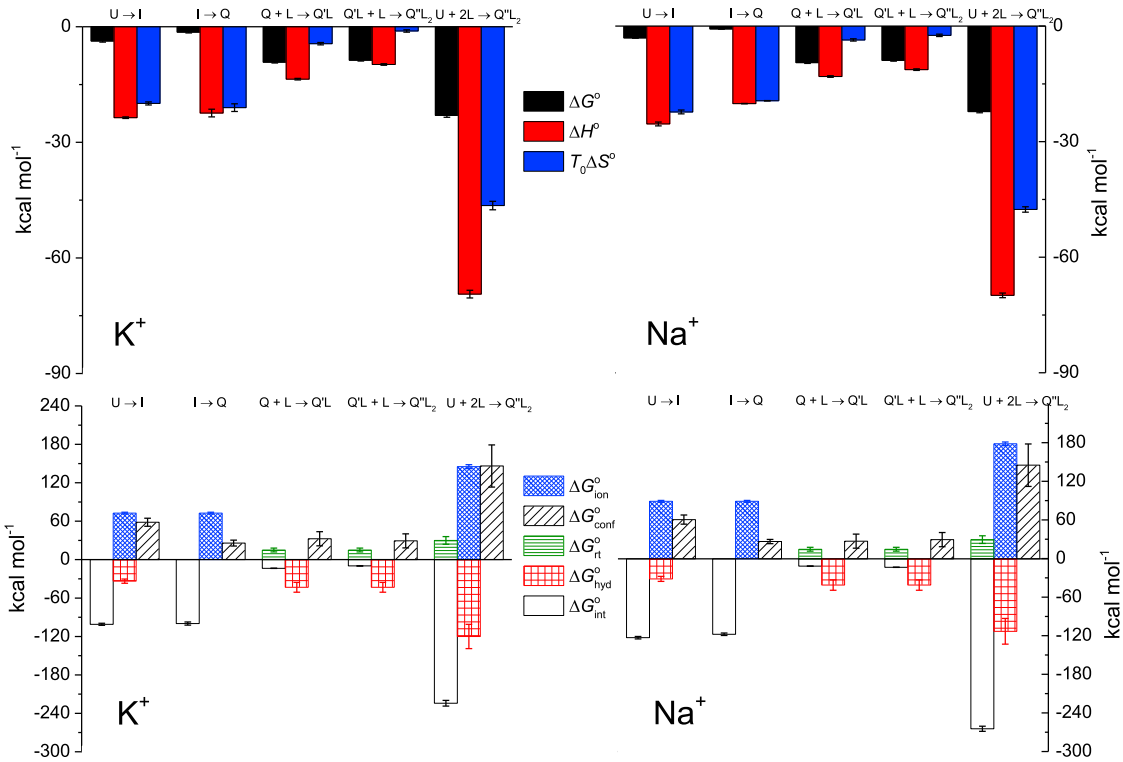

FIGURE 4 Thermodynamic profiles (*top*) and Gibbs free energy contributions (driving forces) for each step in the Tel22 binding-coupled folding mechanism in the presence of ligand (Phen-DC3) and 100 mM K^+ or Na^+ (*bottom*) at 25°C. The errors of ΔG° contributions (Eq. 4) were calculated by combining the errors of experimental quantities (ΔG°, ΔH°, and ΔC°_P; global model analysis) and errors reported in the literature (ΔG°_{ion}, ΔG°_{hyd}, and ΔG°_{rt}) (46,48). To see this figure in color, go online.

$A_{Na^+} + 2L \rightarrow Q''L_{2,Na}{}^+$) events are also accompanied by similar energetic contributions (Fig. 4 and Table S2). Because according to the thermodynamic parameters that characterize unfolding of A_{Na^+} and H_{K^+} (Table S1), the A_{Na^+} and H_{K^+} conformations are energetically very similar, this observation is consistent with the suggested similarity of the ligand-quadruplex structures in the presence of K^+ and Na^+.

Driving forces of binding-induced structural alterations

Several relatively recent articles discuss the thermodynamic forces that may control folding of G-quadruplexes (40–42). We present here, to the best of our knowledge, the first attempt at quantitative dissection of ΔG° accompanying the folding and ligand binding-coupled structural transitions of ht-DNA to more fundamental contributions (Fig. 4 and Table S3). Following the additivity approach (43–45), ΔG° can be treated as a sum of the main contributions,

$$\Delta G^\circ = \Delta G^\circ_{solv} + \Delta G^\circ_{int} + \Delta G^\circ_{rt} + \Delta G^\circ_{conf}, \qquad (4)$$

in which the first contribution, ΔG°_{solv}, ascribed to the solvation effects (reorganization of water molecules surrounding Tel22, ions, and ligands) may be further expressed as $\Delta G^\circ_{solv} = \Delta G^\circ_{ion} + \Delta G^\circ_{hyd}$. The ΔG°_{ion} contribution reflects the dehydration of K^+ or Na^+ ions accompanying their coordinative binding within Tel22. Its enthalpic and entropic origin has been well characterized by Marcus (46) and results in the estimates of $\Delta G^\circ_{ion,K}{}^+ = 72.6$ kcal mol^{-1} and $\Delta G^\circ_{ion,Na}{}^+ = 89.6$ kcal mol^{-1}. The ΔG°_{hyd} contribution is ascribed to the desolvation/solvation of Tel22 and ligand molecules and may be interpreted mainly as a hydrophobic contribution to the overall ΔG° of folding and/or binding (43,44,47). At 25°C it may be estimated by an empirical relation as $\Delta G^\circ_{hyd} = \Delta C^\circ_P \cdot 80(\pm 10)$K (48,49), where ΔC°_P is the corresponding heat capacity change determined by the global model analysis of experimental data (Figs. 2 and S1) combined with the careful treatment of the corresponding baselines (DSC and ITC). The second main contribution, ΔG°_{int}, reflects the specific intra- and intermolecular interactions (van der Waals (base-stacking), H-bonds, Coulombic interactions, and cation coordination) that stabilize a particular Tel22 conformation. It can be considered mainly as an enthalpic contribution and estimated as the difference between the measured enthalpy change, ΔH°, and the corresponding enthalpy of ion dehydration, ΔH°_{ion} (46). Thus, $\Delta G^\circ_{int} \approx \Delta H^\circ - \Delta H^\circ_{ion}$. The third main contribution, ΔG°_{rt}, is considered as an entropic contribution due to changes of rotational and translational freedom of ligand and Tel22 (lost upon ligand binding):

$\Delta G^{\circ}_{rt} = -T\Delta S^{\circ}_{rt}$. Similarly, the fourth main contribution ΔG°_{conf} is interpreted as an entropic contribution accompanying the changes of conformational freedom of Tel22, $\Delta G^{\circ}_{conf} = -T\Delta S^{\circ}_{conf}$. It may be estimated as $\Delta G^{\circ}_{conf} = \Delta G^{\circ} - \Delta G^{\circ}_{solv} - \Delta G^{\circ}_{int} - \Delta G^{\circ}_{rt}$. At this point, we would like to mention that in our dissection of ΔG° the free energy contribution due to the release of the nonspecifically bound cations, which accompanies unfolding of Tel22 and ligand binding to it, has been neglected. Namely, according to the prediction of the polyelectrolyte theory (50), this electrostatic contribution is relatively small (its absolute value is smaller than the error of the least accurate contribution in Eq. 4).

We are well aware that, due to approximations involved in the additivity approach presented above, the interpretation of ΔG° contributions should be taken with great care. It should be emphasized that the main aim of using Eq. 4 is to show the importance of various types of interactions and conformational changes in the formation of folding intermediates and ligand-quadruplex complexes. To demonstrate this, the ΔG° contributions do not need to be specified with high precision (see below). In this light, the described dissection of energetics (Fig. 4) enables us to characterize the dominant driving forces involved in the Tel22 binding-induced structural transitions in the following way:

1) $U \rightarrow I$ transition accompanied by specific binding (dehydration) of one cation appears to be driven by specific interactions and hydrophobic desolvation because $[-(\Delta G^{\circ}_{int} + \Delta G^{\circ}_{hyd}) > (\Delta G^{\circ}_{conf} + \Delta G^{\circ}_{ion})]$. It seems that even though base-stacking, H-bonding, and cation coordination are needed for the early stage of Tel22 secondary structure formation, intermediate states would not be significantly populated without being stabilized by hydrophobic desolvation (if $\Delta G^{\circ}_{hyd} \approx 0 \Rightarrow -(\Delta G^{\circ}_{int} + \Delta G^{\circ}_{hyd}) < (\Delta G^{\circ}_{conf} + \Delta G^{\circ}_{ion}) \Rightarrow \Delta G^{\circ}_{U\rightarrow I} > 0$; I formation unfavorable). Although I_{K^+} and I_{Na^+} are structurally different (Fig. 3), the observation that $\Delta G^{\circ}_{hyd,Na^+} \approx \Delta G^{\circ}_{hyd,K^+}$ suggests that hydrophobic desolvation are equally important for driving the first step of Tel22 folding in Na^+ and K^+ solutions.
2) $I \rightarrow Q$ transition accompanied by specific binding (dehydration) of one cation appears to be driven entirely by specific interactions that overcome loss of conformational freedom and unfavorable ion dehydration $[-\Delta G^{\circ}_{int} > (\Delta G^{\circ}_{conf} + \Delta G^{\circ}_{ion})$; $\Delta G^{\circ}_{hyd} \approx 0]$. The conformational entropy loss is approximately two times lower than in the case of the $U \rightarrow I$ step, which is in accordance with structural properties of I that are closer to Q than to U (Fig. 4). The observation that for the $U \rightarrow I$ and $I \rightarrow Q$ step, $\Delta G^{\circ}_{int,Na^+} < \Delta G^{\circ}_{int,K^+}$, suggests that specific interactions are more favorable for stabilizing I and Q in the presence of Na^+ ions, which can be ascribed to energetically more favorable coordination of Na^+ compared to K^+ ions.
3) $Q + L \rightarrow Q'L$ and $Q'L + L \rightarrow Q''L_2$ steps resulting in the formation of $Q'L$ and $Q''L_2$ conformations that differ from the corresponding ligand-free structures Q are driven predominantly by removal of water from ligand-Tel22 interacting surface, which, together with specific (ligand-Tel22 stacking) interactions, overcome unfavorable loss of conformational, translational, and rotational freedom. Even if we overestimate the magnitude of ΔG°_{rt}, by taking as an approximation $\Delta G^{\circ}_{rt} \approx 15$ kcal mol^{-1} (51,52), the ΔG°_{conf} is still very high (Fig. 4). This means that the $Q + L \rightarrow Q'L$ and $Q'L + L \rightarrow Q''L_2$ steps are accompanied by a large Tel22 conformational entropy loss, which is in accordance with the observed ligand-induced conformational changes (Figs. 3 and S9).

CONCLUSION

The global model analysis of a wide variety of experimental data enabled us to describe the ht-DNA (Tel22) behavior in aqueous solutions at various conditions (temperature, salt, and ligand concentration; Fig. 2 *e*). It resulted in the proposed hierarchy of forces that drive the structural alterations of Tel22 in the absence and presence of G-quadruplex specific ligands, Phen-DC3 and 360A-Br. We believe that such an approach can generally be used in discussing the heterogeneity of both the ht-quadruplex structural polymorphism and its folding and binding pathways.

SUPPORTING MATERIAL

Supporting Materials and Methods, Supporting Results, 11 figures, and five tables are available at http://www.biophysj.org/biophysj/supplemental/S0006-3495(15)00458-0.

AUTHOR CONTRIBUTIONS

J.L. and G.V. designed research; M.B., F.H., and B.I. performed research; M.-P.T.-F. and F.H. contributed new reagents; M.B., J.L., and S.H. analyzed data; and J.L., M.B., G.V., and S.H. wrote the article.

ACKNOWLEDGMENTS

Financial support of the Slovenian Research Agency through grant No. P1-0201 and by COST action No. MP0802 is gratefully acknowledged. J.L. thanks the Excellent NMR - Future Innovation for Sustainable Technologies Centre of Excellence for purchasing the DSC apparatus, which was used to perform this study. M.-P.T.-F thanks Agence Nationale pour la Recherche (ANR), ANR-Gquad, for funding F.H. (postdoctoral fellowship).

REFERENCES

1. Biffi, G., D. Tannahill, …, S. Balasubramanian. 2013. Quantitative visualization of DNA G-quadruplex structures in human cells. *Nat. Chem.* 5:182–186.

2. O'Sullivan, R. J., and J. Karlseder. 2010. Telomeres: protecting chromosomes against genome instability. *Nat. Rev. Mol. Cell Biol.* 11:171–181.
3. Siddiqui-Jain, A., C. L. Grand, …, L. H. Hurley. 2002. Direct evidence for a G-quadruplex in a promoter region and its targeting with a small molecule to repress c-MYC transcription. *Proc. Natl. Acad. Sci. USA.* 99:11593–11598.
4. Zahler, A. M., J. R. Williamson, …, D. M. Prescott. 1991. Inhibition of telomerase by G-quartet DNA structures. *Nature.* 350:718–720.
5. Balasubramanian, S., L. H. Hurley, and S. Neidle. 2011. Targeting G-quadruplexes in gene promoters: a novel anticancer strategy? *Nat. Rev. Drug Discov.* 10:261–275.
6. Parkinson, G. N., M. P. H. Lee, and S. Neidle. 2002. Crystal structure of parallel quadruplexes from human telomeric DNA. *Nature.* 417: 876–880.
7. Ambrus, A., D. Chen, …, D. Yang. 2006. Human telomeric sequence forms a hybrid-type intramolecular G-quadruplex structure with mixed parallel/antiparallel strands in potassium solution. *Nucleic Acids Res.* 34:2723–2735.
8. Phan, A. T., V. Kuryavyi, …, D. J. Patel. 2007. Structure of two intramolecular G-quadruplexes formed by natural human telomere sequences in K^+ solution. *Nucleic Acids Res.* 35:6517–6525.
9. Gray, R. D., L. Petraccone, …, J. B. Chaires. 2010. Characterization of a K^+-induced conformational switch in a human telomeric DNA oligonucleotide using 2-aminopurine fluorescence. *Biochemistry.* 49: 179–194.
10. Luu, K. N., A. T. Phan, …, D. J. Patel. 2006. Structure of the human telomere in K^+ solution: an intramolecular $(3 + 1)$ G-quadruplex scaffold. *J. Am. Chem. Soc.* 128:9963–9970.
11. Wang, Y., and D. J. Patel. 1993. Solution structure of the human telomeric repeat d[AG3(T2AG3)3] G-tetraplex. *Structure.* 1:263–282.
12. Nicoludis, J. M., S. P. Barrett, …, L. A. Yatsunyk. 2012. Interaction of human telomeric DNA with *n*-methyl mesoporphyrin IX. *Nucleic Acids Res.* 40:5432–5447.
13. Rahman, K. M., A. P. Reszka, …, D. E. Thurston. 2009. Biaryl polyamides as a new class of DNA quadruplex-binding ligands. *Chem. Commun. (Camb.).* 27:4097–4099.
14. Granzhan, A., H. Ihmels, and K. Jäger. 2009. Diazonia- and tetraazoniapolycyclic cations as motif for quadruplex-DNA ligands. *Chem. Commun. (Camb.).* 10:1249–1251.
15. Garner, T. P., H. E. L. Williams, …, M. S. Searle. 2009. Selectivity of small molecule ligands for parallel and anti-parallel DNA G-quadruplex structures. *Org. Biomol. Chem.* 7:4194–4200.
16. Chen, M., G. Song, …, X. Qu. 2009. Small-molecule selectively recognizes human telomeric G-quadruplex DNA and regulates its conformational switch. *Biophys. J.* 97:2014–2023.
17. Chu, J. F., T. C. Chang, and H. W. Li. 2010. Single-molecule TPM studies on the conversion of human telomeric DNA. *Biophys. J.* 98:1608–1616.
18. Čeru, S., P. Šket, …, J. Plavec. 2014. A new pathway of DNA G-quadruplex formation. *Angew. Chem. Int.Engl.* 53:4881–4884.
19. Koirala, D., T. Mashimo, …, H. Sugiyama. 2012. Intramolecular folding in three tandem guanine repeats of human telomeric DNA. *Chem. Commun. (Camb.).* 48:2006–2008.
20. Gray, R. D., R. Buscaglia, and J. B. Chaires. 2012. Populated intermediates in the thermal unfolding of the human telomeric quadruplex. *J. Am. Chem. Soc.* 134:16834–16844.
21. Stadlbauer, P., L. Trantírek, …, J. Sponer. 2014. Triplex intermediates in folding of human telomeric quadruplexes probed by microsecond-scale molecular dynamics simulations. *Biochimie.* 105:22–35.
22. Dettler, J. M., R. Buscaglia, …, E. A. Lewis. 2011. DSC deconvolution of the structural complexity of c-MYC P1 promoter G-quadruplexes. *Biophys. J.* 100:1517–1525.
23. Cantor, C. R., M. M. Warshaw, and H. Shapiro. 1970. Oligonucleotide interactions. 3. Circular dichroism studies of the conformation of deoxyoligonucleotides. *Biopolymers.* 9:1059–1077.
24. Bončina, M., J. Lah, …, G. Vesnaver. 2012. Energetic basis of human telomeric DNA folding into G-quadruplex structures. *J. Am. Chem. Soc.* 134:9657–9663.
25. De Cian, A., E. Delemos, …, D. Monchaud. 2007. Highly efficient G-quadruplex recognition by bisquinolinium compounds. *J. Am. Chem. Soc.* 129:1856–1857.
26. Monchaud, D., and M. P. Teulade-Fichou. 2008. A hitchhiker's guide to G-quadruplex ligands. *Org. Biomol. Chem.* 6:627–636.
27. Sidibe, A., F. Hamon, …, J. F. Riou. 2012. Effects of a halogenated G-quadruplex ligand from the pyridine dicarboxamide series on the terminal sequence of XpYp telomere in HT1080 cells. *Biochimie.* 94:2559–2568.
28. Chung, W. J., B. Heddi, …, A. T. Phan. 2014. Solution structure of a G-quadruplex bound to the bisquinolinium compound Phen-DC_3. *Angew. Chem. Int. Ed. Engl.* 53:999–1002.
29. Drobnak, I., G. Vesnaver, and J. Lah. 2010. Model-based thermodynamic analysis of reversible unfolding processes. *J. Phys. Chem. B.* 114:8713–8722.
30. Gavathiotis, E., R. A. Heald, …, M. S. Searle. 2003. Drug recognition and stabilization of the parallel-stranded DNA quadruplex $d(TTAGGGT)_4$ containing the human telomeric repeat. *J. Mol. Biol.* 334:25–36.
31. Parkinson, G. N., F. Cuenca, and S. Neidle. 2008. Topology conservation and loop flexibility in quadruplex-drug recognition: crystal structures of inter- and intramolecular telomeric DNA quadruplex-drug complexes. *J. Mol. Biol.* 381:1145–1156.
32. Mashimo, T., H. Yagi, …, H. Sugiyama. 2010. Folding pathways of human telomeric type-1 and type-2 G-quadruplex structures. *J. Am. Chem. Soc.* 132:14910–14918.
33. Olsen, C. M., W. H. Gmeiner, and L. A. Marky. 2006. Unfolding of G-quadruplexes: energetic, and ion and water contributions of G-quartet stacking. *J. Phys. Chem. B.* 110:6962–6969.
34. Limongelli, V., S. De Tito, …, M. Parrinello. 2013. The G-triplex DNA. *Angew. Chem. Int. Ed. Engl.* 52:2269–2273.
35. Gray, R. D., J. Li, and J. B. Chaires. 2009. Energetics and kinetics of a conformational switch in G-quadruplex DNA. *J. Phys. Chem. B.* 113:2676–2683.
36. Mergny, J. L., A. T. Phan, and L. Lacroix. 1998. Following G-quartet formation by UV-spectroscopy. *FEBS Lett.* 435:74–78.
37. Brandts, J. F., and L.-N. Lin. 1990. Study of strong to ultratight protein interactions using differential scanning calorimetry. *Biochemistry.* 29:6927–6940.
38. De Cian, A., and J. L. Mergny. 2007. Quadruplex ligands may act as molecular chaperones for tetramolecular quadruplex formation. *Nucleic Acids Res.* 35:2483–2493.
39. Buscaglia, R., M. C. Miller, …, J. B. Chaires. 2013. Polyethylene glycol binding alters human telomere G-quadruplex structure by conformational selection. *Nucleic Acids Res.* 41:7934–7946.
40. Lane, A. N., J. B. Chaires, …, J. O. Trent. 2008. Stability and kinetics of G-quadruplex structures. *Nucleic Acids Res.* 36:5482–5515.
41. Smirnov, I. V., and R. H. Shafer. 2007. Electrostatics dominate quadruplex stability. *Biopolymers.* 85:91–101.
42. Gray, R. D., and J. B. Chaires. 2011. Linkage of cation binding and folding in human telomeric quadruplex DNA. *Biophys. Chem.* 159:205–209.
43. Haq, I., J. E. Ladbury, …, J. B. Chaires. 1997. Specific binding of Hoechst 33258 to the d(CGCAAATTTGCG)2 duplex: calorimetric and spectroscopic studies. *J. Mol. Biol.* 271:244–257.
44. Lah, J., and G. Vesnaver. 2004. Energetic diversity of DNA minor-groove recognition by small molecules displayed through some model ligand-DNA systems. *J. Mol. Biol.* 342:73–89.
45. Lah, J., I. Drobnak, …, G. Vesnaver. 2008. What drives the binding of minor groove-directed ligands to DNA hairpins? *Nucleic Acids Res.* 36:897–904.
46. Marcus, Y. A. 1986. Ion Solvation. John Wiley, New York.

47. Majhi, P. R., J. Qi, …, R. H. Shafer. 2008. Heat capacity changes associated with guanine quadruplex formation: an isothermal titration calorimetry study. *Biopolymers.* 89:302–309.

48. Baldwin, R. L. 1986. Temperature dependence of the hydrophobic interaction in protein folding. *Proc. Natl. Acad. Sci. USA.* 83:8069–8072.

49. Spolar, R. S., and M. T. Record, Jr. 1994. Coupling of local folding to site-specific binding of proteins to DNA. *Science.* 263:777–784.

50. Record, Jr., M. T., C. F. Anderson, and T. M. Lohman. 1978. Thermodynamic analysis of ion effects on the binding and conformational equilibria of proteins and nucleic acids: the roles of ion association or release, screening, and ion effects on water activity. *Q. Rev. Biophys.* 11:103–178.

51. Finkelstein, A. V., and J. Janin. 1989. The price of lost freedom: entropy of bimolecular complex formation. *Protein Eng.* 3:1–3.

52. Dolenc, J., R. Baron, …, W. F. van Gunsteren. 2006. Configurational entropy change of netropsin and distamycin upon DNA minor-groove binding. *Biophys. J.* 91:1460–1470.

Supporting Information

Dominant driving forces in human telomere quadruplex binding-induced structural alterations

Matjaz Boncina,[1] Florian Hamon,[2] Barira Islam,[3] Marie-Paule Teulade-Fichou,[2] Gorazd Vesnaver,[1] Shozeb Haider,[3,4] and Jurij Lah[1,*]

[1]Faculty of Chemistry and Chemical Technology, University of Ljubljana, Večna pot 113, SI–1000 Ljubljana, Slovenia.

[2]Institut Curie, CNRS UMR-176, Centre Universitaire d'Orsay, Paris-Sud 91405 Orsay Cedex France.

[3]Centre for Cancer Research and Cell Biology, Queen's University of Belfast, Belfast BT9 7BL, UK.

[4]UCL School of Pharmacy 29-39 Brunswick Square, Bloomsbury, London WC1N 1AX, UK.

*Corresponding author footnote:
Jurij Lah
Faculty of Chemistry and Chemical Technology, University of Ljubljana, SI–1000 Ljubljana, Slovenia.
E-mail: jurij.lah@fkkt.uni-lj.si

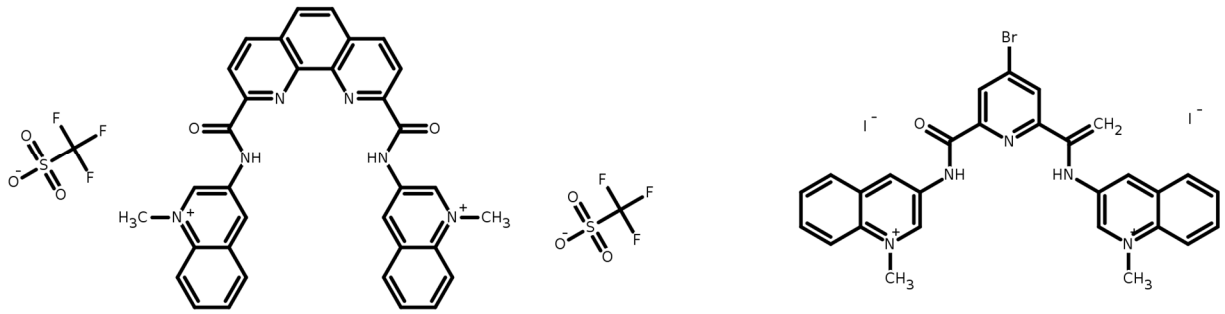

FIGURE S1 Bisquinolinium ligands used in this study: The Phenanthroline Dicarboxamide derivative Phen-DC3 (left), and the Bromo-Pyridine Dicarboxamide derivative 360A-Br.

METHODS

Model Based Analysis of Experimental Data

The simplest model mechanism of ion and ligand binding-coupled folding of Tel22, that successfully describes the corresponding calorimetric and spectroscopic data obtained in solutions with K^+ or Na^+, ions involves five macroscopic states: U (unfolded DNA), I (intermediate), Q (folded G-quadruplex), Q'L and Q''L_2 (folded G-quadruplex with one and two bound ligand molecules).

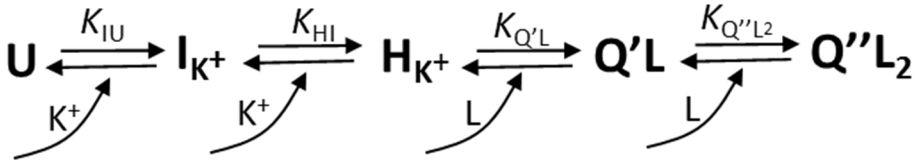

FIGURE S2 Schematic presentation of the simplest equilibrium model of ion- and ligand (L)-induced Tel22 structural transitions in the presence of K^+ ions (see also Scheme 1 in the main text) that at various temperatures and salt concentrations assumes inter-conversions between the unfolded (U), the intermediate (I), the folded G-quadruplex structure (Q), and the quadruplex complexes with one or two bound ligand molecules (Q'L, Q''L_2).

For a given model one can write a general equation for the measured spectroscopic and calorimetric properties of the ion-ligand-DNA solution (Eq.1) from which the corresponding contributions of the buffer are subtracted. Such property, *X*, can be presented as a linear

combination of molar ratios, $\alpha_j = [c_j]/c_{DNA}$ of all species, j, present in the solution (j = L, U, I, Q, Q'L, Q''L_2)

$$X = X_L\alpha_L + X_U\alpha_U + X_I\alpha_I + X_Q\alpha_Q + X_{Q'L}\alpha_{Q'L} + X_{Q''L_2}\alpha_{Q''L_2} \quad (1)$$

where X_j represents the property of the solute j at a given pressure, P, temperature, T, salt type (KCl, NaCl), salt concentration and the total DNA concentration, c_{DNA}. Since according to the model $\alpha_U + \alpha_I + \alpha_Q + \alpha_{Q'L} + \alpha_{Q''L_2} = 1$ and $\alpha_L + \alpha_{Q'L} + 2\alpha_{Q''L_2} = r$ where $r = c_{L,tot} / c_{DNA} = n_{L,tot} / n_{DNA}$ ($c_{L,tot}$ is the total ligand concentration) one obtains

$$X = X_L r + (\Delta X_{IU} + \Delta X_{QI})\alpha_U + \Delta X_{QI}\alpha_I + X_Q + \Delta X_{Q'L}\alpha_{Q'L} + (\Delta X_{Q'L} + \Delta X_{Q''L_2})\alpha_{Q''L_2} \quad (2)$$

where the changes $\Delta X_{IU} = X_U - X_I$, $\Delta X_{QI} = X_I - X_Q$, $\Delta X_{Q'L} = X_{Q'L} - X_Q - X_L$, $\Delta X_{Q''L_2} = X_{Q''L_2} - X_{Q'L} - X_L$ refer to each step in the model mechanism (Fig. S2).

Unfolding/folding of Human Telomeric DNA in the Absence of Ligand

Folding/unfolding process [U ↔ I ↔ Q] of Tel22, in the presence of Na^+ or K^+ ions (no ligand present) was studied using differential scanning calorimetry (DSC) and CD spectroscopy. Experimental data obtained for Tel22 in KCl and NaCl solutions were analyzed using the three-state equilibrium model (1). In the DSC experiments the measured quantity is the partial molar heat capacity of DNA, $\overline{C}_{P,DNA}$. In the further analysis $\overline{C}_{P,DNA}$ is more conveniently expressed as the excess heat capacity, $\Delta C_P = \overline{C}_{P,DNA} - \overline{C}_{P,int}$ where $\overline{C}_{P,int}$ represents an intrinsic heat capacity of DNA formally defined as $\overline{C}_{P,int} = \alpha_Q\overline{C}_{P,Q} + \alpha_I\overline{C}_{P,I} + \alpha_U\overline{C}_{P,U}$. In the measured temperature interval, $\overline{C}_{P,int}$ was approximated by the second order polynomial on T, fitted to the low-temperature (folded form) and high-temperature (unfolded form) parts of the experimental $\overline{C}_{P,DNA}$, and then subtracted from $\overline{C}_{P,DNA}$ to obtain ΔC_P. This approach has already been described in detail in SI of ref 1. The excess heat capacity, ΔC_P, determined by DSC can also be calculated for the suggested model

from the temperature derivative of Eq. 2 for $X = H$ at constant pressure P. Since all experiments were performed at very low concentrations where $\Delta C_{P,\mathrm{ij}} = \Delta C^{\circ}_{P,\mathrm{ij}}$ and $\Delta H_{\mathrm{ij}} = \Delta H^{\circ}_{\mathrm{ij}}$ one obtains

$$\Delta C^{\circ}_{P} = (\partial \alpha_{\mathrm{U}} / \partial T)(\Delta H^{\circ}_{\mathrm{IU}} + \Delta H^{\circ}_{\mathrm{QI}}) + (\partial \alpha_{\mathrm{I}} / \partial T)\Delta H^{\circ}_{\mathrm{QI}} \tag{3}$$

where $\Delta H^{\circ}_{\mathrm{IU}}$ and $\Delta H^{\circ}_{\mathrm{QI}}$ are the standard enthalpies of I → U and Q → I transition, respectively. The measured CD spectra may be described in a similar way. In this case the quantity X in Eq. 1 represents, [Θ], that is the measured ellipticity at a given wavelength, Θ, divided by the optical path length, l, and the total DNA concentration, c_{DNA}. By taking into account that the molar ellipticities of G-quadruplex in the folded, $[\Theta]_{\mathrm{Q}}$, and unfolded, $[\Theta]_{\mathrm{U}}$, state can be obtained by extrapolation of [Θ] from pre-, $[\Theta]_{\mathrm{Q}}$, and post-, $[\Theta]_{\mathrm{U}}$, transitional parts of the unfolding curves and that $\alpha_{\mathrm{Q}} = 1 - \alpha_{\mathrm{I}} - \alpha_{\mathrm{U}}$ one can express the experimentally obtained induced signal f in terms of the model function (1).

$$f = \frac{[\Theta] - [\Theta]_{\mathrm{Q}}}{[\Theta]_{\mathrm{U}} - [\Theta]_{\mathrm{Q}}} = \alpha_{\mathrm{I}} f_{\mathrm{QI}} + \alpha_{\mathrm{U}} \tag{4}$$

in which f_{QI} can be considered as the temperature independent normalization coefficient.

Binding of the Ligands to Human Telomeric DNA

In order to study binding of the selected ligands to Tel22 in buffer solutions we have to make sure that the ligands are soluble and that the formed ligand-DNA complexes do no aggregate. These problems were overcome by dissolving the ligands in buffer solution containing 3% DMSO and by titrating DNA solution containing 3% DMSO into the ligand solution. The choice of DMSO was based on the experimental evidence that up to 5% DMSO has practically no effect on the thermodynamic quantities of binding (2,3). The ligand binding experiments were performed at conditions (T, salt concentration) where only intermediate (I) and folded G-quadruplex (Q) conformations were present at the beginning of the experiment, but not the unfolded DNA ($\alpha_{\mathrm{U}} = 0$).

In the case of CD titrations the quantity X in Eq. 2 is at any titration point presented as [Θ], that is the measured ellipticity, Θ, at a given wavelength divided by the optical path length, l, and the total DNA concentration, c_{DNA}. By subtracting molar ellipticity of the folded G-quadruplex, $[\Theta]_Q$, and taking into account that the unbound ligands are not optically active ($[\Theta]_L = 0$) one obtains a relation between the experimentally obtained induced signal Δ[Θ] (left-hand side of Eq. 5) and the model function (right-hand side of Eq. 5)

$$\Delta[\Theta] = [\Theta] - [\Theta]_Q = \Delta[\Theta]_{QI}\,\alpha_I + \Delta[\Theta]_{Q'L}\,\alpha_{Q'L} + \left(\Delta[\Theta]_{Q'L} + \Delta[\Theta]_{Q''L_2}\right)\alpha_{Q''L_2} \tag{5}$$

Similarly, in the case of fluorimetry the quantity X in Eq. 2 represents normalized measured emitted fluorescence, $X=[F]=I_F/(c_{DNA}l)$. By subtracting the normalized fluorescence that ligand would have at the same total ligand concentration in the absence of DNA, $[F]_L \cdot r$, and by taking into account that DNA itself does not emit fluorescence ($[F]_Q = 0$, $\Delta[F]_{QI} = 0$) one obtains

$$\Delta[F] = [F] - [F]_L\, r = \Delta[F]_{Q'L}\,\alpha_{Q'L} + \left(\Delta[F]_{Q'L} + \Delta[F]_{Q''L_2}\right)\alpha_{Q''L_2} \tag{6}$$

In the case of ITC, the quantity X in Eq. 2 represents H_m, that is, the enthalpy of solution in the measuring cell expressed per mole of DNA from which the corresponding enthalpy of solvent S (buffer solution) is subtracted

$$H_m = \bar{H}_L r + \Delta H_{QI}\alpha_I + \bar{H}_Q + \Delta H_{Q'L}\alpha_{Q'L} + \left(\Delta H_{Q'L} + \Delta H_{Q''L_2}\right)\alpha_{Q''L_2} \tag{7}$$

$\bar{H}_L$ and $\bar{H}_Q$ are the partial molar enthalpies of ligand and the folded G-quadruplex, and ΔH_{QI}, $\Delta H_{Q'L}$ and $\Delta H_{Q''L_2}$ are the enthalpies of Q → I, Q → Q'L and Q'L → Q''L_2 transitions, respectively. By multiplying Eq. 7 with the total amount of the DNA, n_{DNA}, taking the partial derivative of this expression with respect to n_{DNA} at P, T, n_S, $n_{L,tot}$ = const. and using the Gibbs-Duhem relation one

obtains an expression for the partial molar enthalpy of the DNA, $\bar{H}_{\mathrm{DNA}}$, which at very low concentrations, where $\bar{H}_{\mathrm{i}} = \bar{H}_{\mathrm{i}}^{\mathrm{o}}$ and $\bar{H}_{\mathrm{ij}} = \bar{H}_{ij}^{\mathrm{o}}$, becomes

$$\bar{H}_{\mathrm{DNA}} = \Delta H_{\mathrm{QI}}^{\mathrm{o}} \left(\partial n_{\mathrm{I}} / \partial n_{\mathrm{DNA}}\right)_{P,T,n_{\mathrm{S}},n_{\mathrm{L,tot}}} + \bar{H}_{\mathrm{Q}}^{\mathrm{o}} + \Delta H_{\mathrm{Q'L}}^{\mathrm{o}} \left(\partial n_{\mathrm{Q'L}} / \partial n_{\mathrm{DNA}}\right)_{P,T,n_{\mathrm{S}},n_{\mathrm{L,tot}}} + \left(\Delta H_{\mathrm{Q'L}}^{\mathrm{o}} + \Delta H_{\mathrm{Q''L_2}}^{\mathrm{o}}\right)\left(\partial n_{\mathrm{Q''L_2}} / \partial n_{\mathrm{DNA}}\right)_{P,T,n_{\mathrm{S}},n_{\mathrm{L,tot}}} \tag{8}$$

Each $(\partial n_{\mathrm{j}} / \partial n_{\mathrm{DNA}})$ term (j = I, Q'L, Q''L_2) in Eq. 8 represents the corresponding partial derivative at n_{DNA} at P, T, n_{S}, $n_{\mathrm{L,tot}}$ = const. which can be further expressed analytically in terms of α_{j} ($\alpha_{\mathrm{j}} = n_{\mathrm{j}}/n_{\mathrm{DNA}}$). In order to obtain enthalpy changes resulting from complex formation, ΔH_T, one needs to perform the blank titration experiment, that is the titration of DNA into the ligand free buffer solution. From Eq. 8 we obtain $\left(\bar{H}_{\mathrm{DNA}}\right)_{\mathrm{bl}} = \Delta H_{\mathrm{QI}}^{\mathrm{o}} \left(\partial n_{\mathrm{I}} / \partial n_{\mathrm{DNA}}\right) + \bar{H}_{\mathrm{Q}}^{\mathrm{o}}$ at P, T, n_{S}, $n_{\mathrm{L=0}}$ = const. and by subtracting this expression from Eq. 8 one obtains the quantity of interest, ΔH_T

$$\begin{aligned}\Delta H_T = \bar{H}_{\mathrm{DNA}} - \left(\bar{H}_{\mathrm{DNA}}\right)_{\mathrm{bl}} = \Delta H_{\mathrm{Q'L}}^{\mathrm{o}} \left(\partial n_{\mathrm{Q'L}} / \partial n_{\mathrm{DNA}}\right)_{P,T,n_{\mathrm{S}},n_{\mathrm{L,tot}}} + \left(\Delta H_{\mathrm{Q'L}}^{\mathrm{o}} + \Delta H_{\mathrm{Q''L_2}}^{\mathrm{o}}\right)\left(\partial n_{\mathrm{Q''L_2}} / \partial n_{\mathrm{DNA}}\right)_{P,T,n_{\mathrm{S}},n_{\mathrm{L,tot}}} \\ + \Delta H_{\mathrm{QI}}^{\mathrm{o}} \left(\left(\partial n_{\mathrm{I}} / \partial n_{\mathrm{DNA}}\right)_{P,T,n_{\mathrm{S}},n_{\mathrm{L,tot}}} - \left(\partial n_{\mathrm{I}} / \partial n_{\mathrm{DNA}}\right)_{P,T,n_{\mathrm{S}},n_{\mathrm{L=0}}}\right)\end{aligned} \tag{9}$$

Global Model Analysis of Experimental Data

Model functions (Eqs. 3-6, 9) resulting from the suggested model (Figure S2, Scheme 1 – main text) were used to describe CD, FL, ITC and DSC data as presented in the main text on page 6.

RESULTS

The "best fit" thermodynamic parameters describing folding/unfolding of Tel22 in the presence of K^+ and Na^+ ions at T_0 = 298.15 K obtained by the semi-global analysis of DSC and CD data (Eqs. 3, 4) are presented in Table S1 and Fig. S3.

As already mentioned, ligands were dissolved in buffer solution containing 3% DMSO, therefore also DNA was prepared in the same solution. In order to examine the effect of DMSO on thermodynamics of folding/unfolding of Tel22 we performed a series of DSC and CD experiments in pure aqueous and 3% DMSO solutions in the presence of K^+ ions (100 mM KCl)

and globally analyzed them with the same model. The comparison of results obtained for both types of solutions clearly shows that the presence of 3 % of DMSO in aqueous solutions has negligible effect on the thermodynamics of Tel22 folding/unfolding processes. Consequently, for description of thermodynamics of folding/unfolding of Tel22 in 3% DMSO solutions in the presence of 100 mM or 200 mM NaCl or KCl the corresponding thermodynamic parameters obtained in DMSO free aqueous solutions were used.

TABLE S1 The "best fit" thermodynamic parameters accompanying folding of Tel22 in Na^+ and K^+ solutions in the absence of ligand at T_0 = 25 °C K obtained by the global three-state model (Eqs. 3, 4) analysis of DSC and CD data.

	100 mM Na^+		100 mM K^+	
	U → I	I → Q	U → I	I → Q
$\Delta G^{o}_{T_0,X^+}$ / kcal mol^{-1}	-3.1±0.1	-0.7±0.1	-3.7±0.1	-1.4±0.1
$\Delta H^{o}_{T_0}$ / kcal mol^{-1}	-25.4±1.0	-20.1±0.2	-23.6±0.6	-22.4±0.1
$T\Delta S^{o}_{T_0,X^+}$ / kcal mol^{-1}	-22.3±1.0	-19.4±0.2	-19.9±0.6	-21.0±0.1
ΔC^{o}_{P} / cal mol^{-1} K^{-1}	-390±30	0±10	-420±20	0±20

Errors represent 2x standard deviations obtained as square roots of diagonal elements of the corresponding variance-covariance matrixes. For comparative purposes $\Delta G^{o}_{T_0}$ was extrapolated from [X^+] = 1 M (best fit parameter value) to [X^+] = 100 mM (this table) by using Eq. 3 – main text.

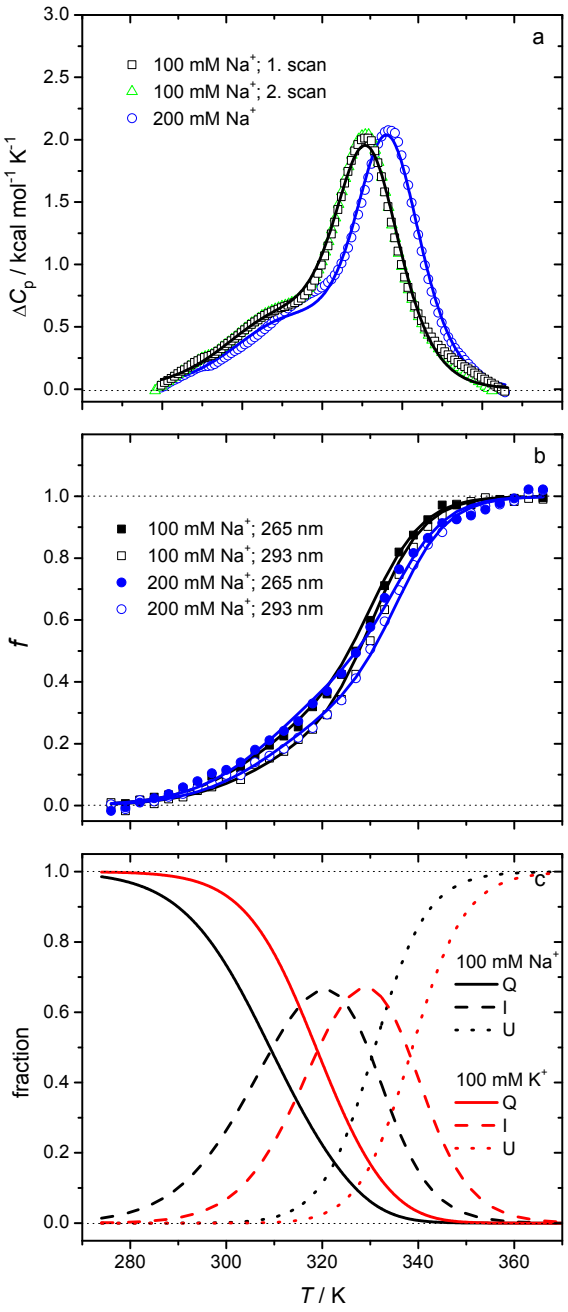

FIGURE S3 Global analysis of the DSC thermograms and CD melting curves measured at different concentrations of Na^+ ions in cacodylic buffer, pH = 6.9, in the absence of ligand.

a) DSC thermograms of Tel22 at different Na^+ concentrations. Experimental data are presented by symbols while the lines refer to the corresponding best global fit of the model function (Eq. 3). DSC thermograms are reproducible in the presence of Na^+ or K^+ (typical 1. and 2. scan for Na^+ are presented) suggesting that folding/unfolding of Tel22 in the presence of ions may be considered as a reversible process. For clarity reasons only every 10th experimental point is shown.

b) Normalized CD melting curves at 265 and 293 nm. Experimental data are presented by symbols while the corresponding best global fit of the model function (Eq. 4) is presented by the lines.

c) The model-predicted fractions of species Q, I and U as a function of *T* in 100 mM Na^+ and 100 mM K^+ determined using the "best fit" parameters reported in Table S1.

TABLE S2 The "best fit" thermodynamic parameters describing binding of Phen-DC3 and 360A-Br to Tel22 at T_0 = 25 °C in the presence of 100 mM Na^+ or 100 mM K^+ ions obtained from global fitting of the model functions (Eqs. 5, 6, 9) to the CD, FL and ITC data presented in Figs. S4-S7.

	Phen-DC3		360A-Br	
	100 mM Na^+	100 mM K^+	100 mM Na^+	100 mM K^+
$K_{Q'L}$	$8.8\cdot10^6$	$5.5\cdot10^6$	$5.3\cdot10^6$	$3.2\cdot10^6$
$\Delta G^o_{Q'L(T_0,X^+)}$ / kcal mol^{-1}	-9.5±0.4	-9.2±0.4	-9.2±0.4	-8.9±0.4
$\Delta H^o_{Q'L(T_0)}$ / kcal mol^{-1}	-13.1±0.4	-13.6±0.4	-15.1±0.6	-15.0±0.6
$T_0\Delta S^o_{Q'L(T_0,X^+)}$ / kcal mol^{-1}	-3.6±0.6	-4.4±0.6	-5.9±0.7	-6.1±0.7
$K_{Q''L_2}$	$3.3\cdot10^6$	$2.2\cdot10^6$	$1.6\cdot10^6$	$6.1\cdot10^5$
$\Delta G^o_{Q''L_2(T_0,X^+)}$ / kcal mol^{-1}	-8.9±0.4	-8.7±0.4	-8.5±0.4	-7.9±0.4
$\Delta H^o_{Q''L_2(T_0)}$ / kcal mol^{-1}	-11.3±0.4	-9.8±0.4	-16.4±0.6	-17.2±0.6
$T_0\Delta S^o_{Q''L_2(T_0,X^+)}$ / kcal mol^{-1}	-2.4±0.6	-1.2±0.6	-7.9±0.7	-9.3±0.7
$\Delta C^o_{P,Q'L} = \Delta C^o_{P,Q''L_2}$ / cal mol^{-1} K^{-1}	-510±60	-540±60	-400±60	-300±60
$\Delta n_{Q'L} = \Delta n_{Q''L_2}$	1.3±0.4	1.5±0.2	1.2±0.2	1.2±0.2
	U → Q'L	U → Q'L	U → Q'L	U → Q'L
$\Delta G^o_{i(T_0,X^+)}$ / kcal mol^{-1}	-13.3±0.4	-14.3±0.4	-13.0±0.4	-14.0±0.4
$\Delta H^o_{i(T_0,X^+)}$ / kcal mol^{-1}	-58.6±1.0	-59.6±0.7	-60.6±1.2	-61.0±0.8
$T_0\Delta S^o_{i(T_0,X^+)}$ / kcal mol^{-1}	-45.3±1.1	-45.3±0.9	-47.6±1.3	-47.0±0.9
	U → Q''L_2	U → Q''L_2	U → Q''L_2	U → Q''L_2
$\Delta G^o_{i(T_0,X^+)}$ / kcal mol^{-1}	-22.2±0.6	-23.0±0.6	-21.5±0.6	-21.9±0.6
$\Delta H^o_{i(T_0,X^+)}$ / kcal mol^{-1}	-69.9±1.1	-69.4.0±0.8	-77.0±1.3	-78.2±1.0
$T_0\Delta S^o_{i(T_0,X^+)}$ / kcal mol^{-1}	-47.6±1.3	-46.4±1.0	-55.5±1.4	-56.3±1.2

Errors represent 2x standard deviations obtained as square roots of diagonal elements of the corresponding variance-covariance matrixes.

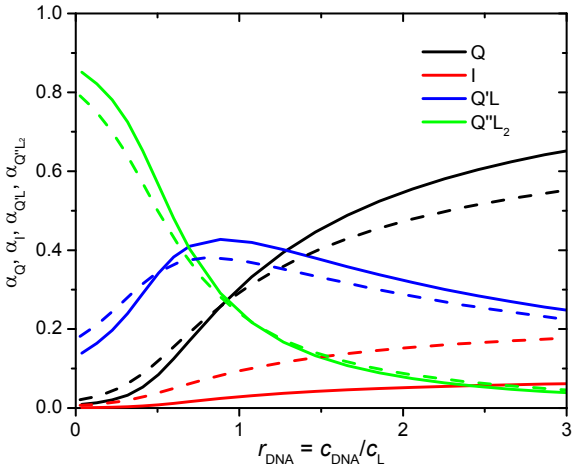

FIGURE S4 Binding of Phen-DC3 on Tel22 in the presence of K^+ ions. The model-predicted fractions of species Q, I, Q'L and Q''L_2 at 25 (solid lines) and 35 (dashed lines) °C and 100 mM K^+ as a function of molar ratio $r_{DNA} = c_{DNA}/c_L$ determined using the "best fit" parameters reported in Table S2.

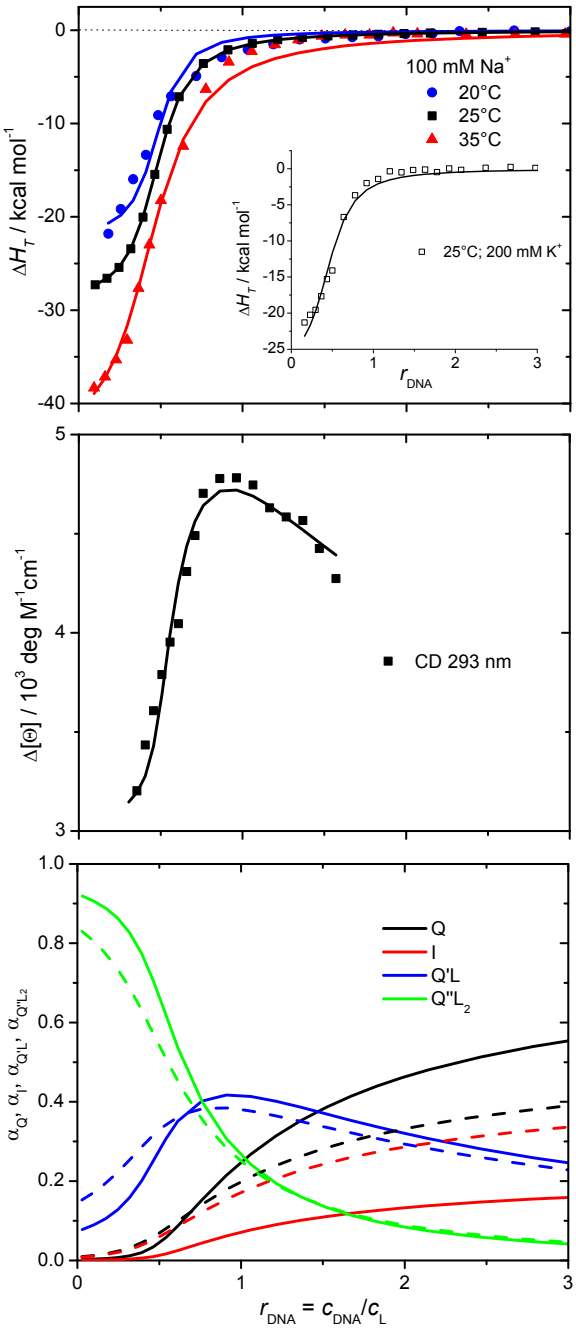

FIGURE S5 Binding of Phen-DC3 on Tel22 in the presence of Na^+ ions. Global analysis of the ITC and CD binding data measured at different *T* and different concentrations of Na^+ ions. Experimental ITC data are presented by symbols, while the lines refer to the corresponding best global fit of the model function (Eq. 9).

Experimental CD-titration data measured at 25°C in the presence of 100 mM Na^+ ions are presented by symbols while the corresponding best global fit of the model function (Eq. 5) is presented by the line.

The model-predicted fractions of species Q, I, Q'L and Q''L_2 at 25 (solid lines) and 35 (dashed lines) °C and 100 mM Na^+ as a function of molar ratio $r_{DNA} = c_{DNA}/c_L$ determined using the "best fit" parameters reported in Table S2.

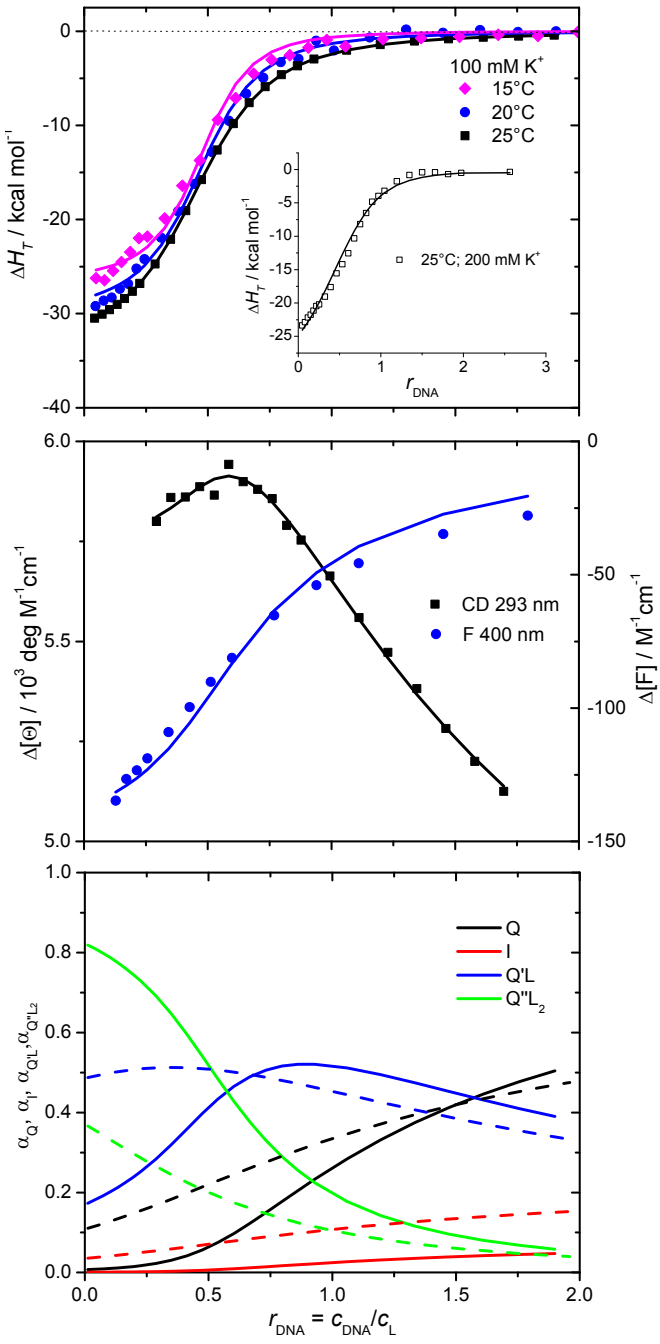

FIGURE S6 Binding of 360A-Br on Tel22 in the presence of K^+ ions. Global analysis of the ITC, CD and FL binding data measured at different *T* and different concentrations of K^+ ions. Experimental ITC data are presented by symbols, while the lines refer to the corresponding best global fit of the model function (Eq. 9).

Experimental CD- and FL-titration data measured at 25°C in the presence of 100 mM K^+ ions are presented by symbols while the corresponding best global fit of the model function (Eqs. 5 and 6) is presented by the lines.

The model-predicted fractions of species Q, I, Q'L and Q''L_2 at 25 (solid lines) and 35 (dashed lines) °C and 100 mM K^+ as a function of molar ratio $r_{DNA} = c_{DNA}/c_L$ determined using the "best fit" parameters reported in Table S2.

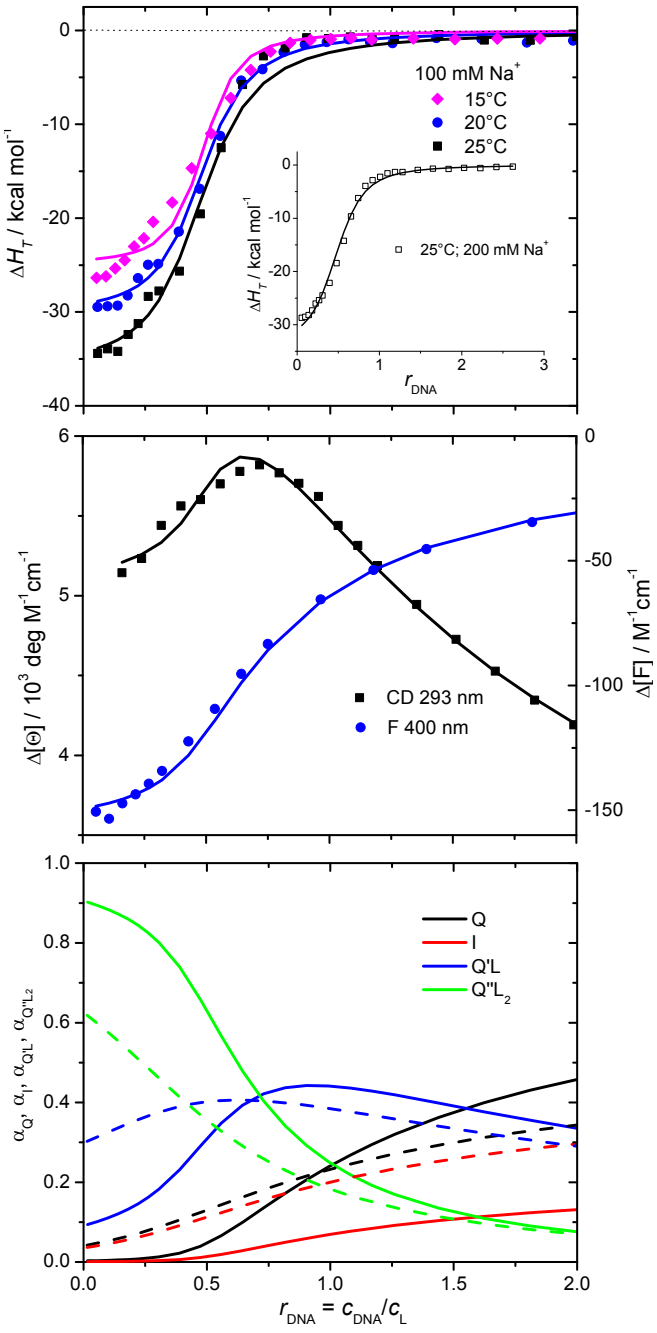

FIGURE S7 Binding of 360A-Br on Tel22 in the presence of Na^+ ions. Global analysis of the ITC, CD and FL binding data measured at different *T* and different concentrations of Na^+ ions. Experimental ITC data are presented by symbols, while the lines refer to the corresponding best global fit of the model function (Eq. 9).

Experimental CD- and FL-titration data measured at 25°C in the presence of 100 mM Na^+ ions are presented by symbols while the corresponding best global fit of the model function (Eqs. 5 and 6) is presented by the lines.

The model-predicted fractions of species Q, I, Q'L and Q''L_2 at 25 (solid lines) and 35 (dashed lines) °C and 100 mM Na^+ as a function of molar ratio $r_{DNA} = c_{DNA}/c_L$ determined using the "best fit" parameters reported in Table S2.

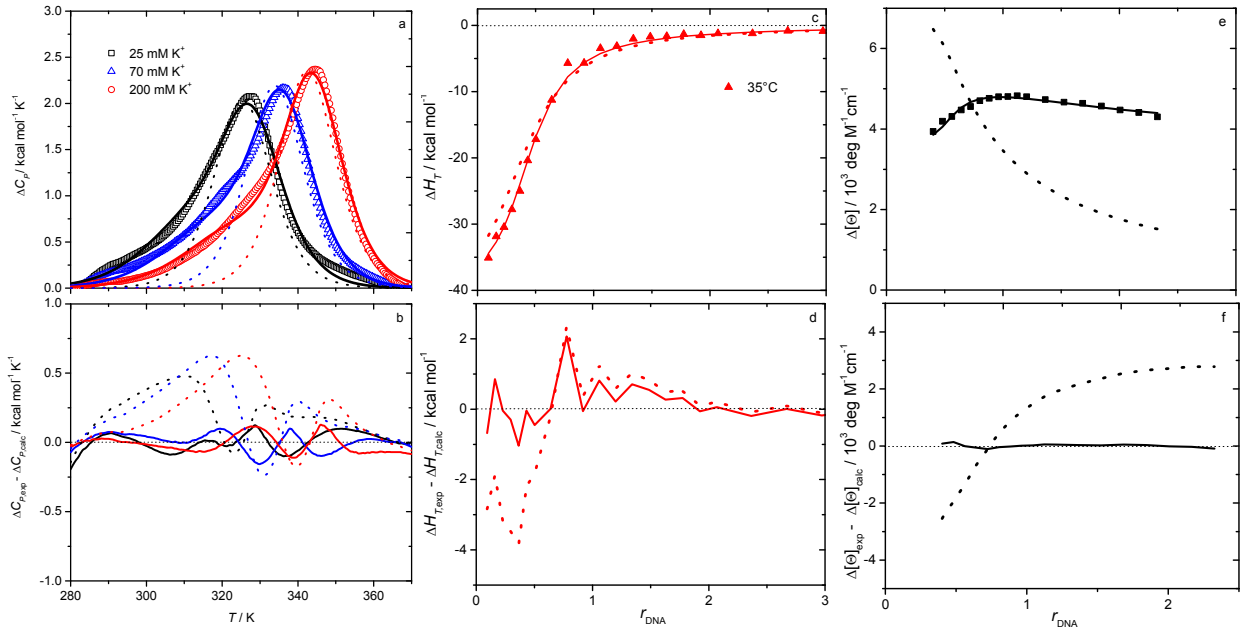

FIGURE S8 Comparison of some characteristic of global fit of the Model 1, Model 2 and Model 3 to the data presented in Fig. 1 of the main text. (a) DSC thermograms: Tel22 at different K^+ concentrations. Experimental data are presented by symbols, the solid lines refer to the corresponding best global fit of the three-state model function (U ↔ I ↔ Q + L ↔ Q'L + L ↔ Q''L_2, Model 1) and the dotted lines to the corresponding best global fit of the two-state model function (U ↔ Q+ L ↔ Q'L + L ↔ Q''L_2, Model 2) in ligand free solution. (b) Differences between experimental ΔC_P values and those calculated by the Model 1 (solid lines) or the Model 2 (dotted lines). (c) ITC titration of Phen-DC3 to Tel22 at 35 °C: Model 2 fits worse (dotted line) the measured ligand binding data (symbols) if the model predicted population of I is not taken into account (at 35 °C the population of I changes for about 20 %; see Figs. S4-S7). (d) Differences between experimental ΔH_T values (symbols) and calculated from the Model 1 (solid line) and Model 2 (dotted line) for binding of Phen-DC3 to Tel22 at 35 °C. (e) CD titration of Phen-DC3 to Tel22 at 25 °C and 293 nm: Model 3 (binding steps described in terms of two identical independent binding sites model) fits worse (dotted line) the measured ligand binding data (symbols) as Model 1 (solid line). (f) Differences between experimental Δ[θ] values (symbols) and calculated from Model 1 (solid line) and Model 3 (dotted line) for binding of Phen-DC3 to Tel22 at 25 °C.

TABLE S3 Dissection of Gibbs free energy changes (Eq. 4 – main text) for each model predicted step (Scheme 1 - main text) at 25 °C and 100 mM Na^+ or K^+ (L = Phen-DC3).

Na^+	$\Delta G°_{solv}$ / kcal mol^{-1}		$\Delta G°_{int}$ / kcal mol^{-1}	$\Delta G°_{rt}$ / kcal mol^{-1}	$\Delta G°_{conf}$ / kcal mol^{-1}
	$\Delta G°_{ion}$	$\Delta G°_{hyd}$			
U → I	90 ± 1	–31 ± 4	–123 ± 2	0	61 ± 7
I → Q	90 ± 1	0	–117 ± 2	0	27 ± 3
Q + L → Q'L	0	–41 ± 8	–11.3 ± 0.2	15 ± 3	28 ± 11
Q'L + L → Q''L_2	0	–41 ± 8	–13.1 ± 0.2	15 ± 3	30 ± 11
U + 2L → Q''L_2	179 ± 3	–113 ± 20	–265 ± 4	30 ± 6	146 ± 33
K^+					
U → I	73 ± 1	–34 ± 3	–101 ± 2	0	58 ± 6
I → Q	73 ± 1	0	–99.8 ± 2	0	26 ± 5
Q + L → Q'L	0	–43 ± 8	–13.6 ± 0.2	15 ± 3	33 ± 11
Q'L + L → Q''L_2	0	–43 ± 8	–9.8 ± 0.2	15 ± 3	29 ± 11
U + 2L → Q''L_2	145 ± 3	–120 ± 19	–224 ± 4	30 ± 6	146 ± 33

$\Delta G°_{ion,Na+}$ = 89.6 kcal mol^{-1} (4)
$\Delta H°_{ion,Na+}$ = 97.3 kcal mol^{-1} (4)
$\Delta G°_{ion,K+}$ = 72.6 kcal mol^{-1} (4)
$\Delta H°_{ion,K+}$ = 77.4 kcal mol^{-1} (4)
$\Delta G°_{hyd} = \Delta C°_P \cdot 80(\pm 10)$K;(5) $\Delta C°_P$ is the experimentally determined value, (see Tables S1 and S2).
$\Delta G°_{int} = \Delta H° - \Delta H°_{ion}$
$\Delta G°_{rt} = -T\Delta S°_{rt}$; $T\Delta S°_{rt}$ = −15 kcal mol^{-1} (6)
$\Delta G°_{conf} = \Delta G° - \Delta G°_{solv} - \Delta G°_{int} - \Delta G°_{rt}$; $\Delta G°$ is the experimentally determined value, (see Tables S1 and S2).
The errors of $\Delta G°$ contributions (Eq. 4 – main text) were calculated combining the errors of experimental quantities ($\Delta G°$, $\Delta H°$, $\Delta C°_P$; global model analysis) and errors reported in the literature ($\Delta G°_{ion}$, $\Delta G°_{hyd}$, $\Delta G°_{rt}$) (4,5,6).

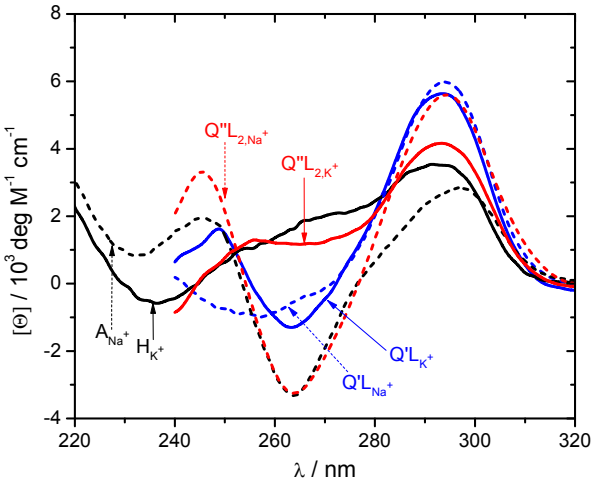

FIGURE S9 CD spectra corresponding to Tel22 antiparallel (A_{Na}+) and hybrid (H_K+) quadruplex structures and complexes with one (Q'L) and two bound ligands (Q''L_2) at 25 °C in the presence of 100 mM K^+ (full lines) or Na^+ (dashed lines) ions and ligand 360A-Br. CD spectra of the complexes were calculated by deconvolution of the measured spectra based on model-predicted populations of species (Figs. S3, S6 and S7) and spectra of Q (A_{Na}+ or H_K+) and I (I_{Na}+ or I_K+) form.

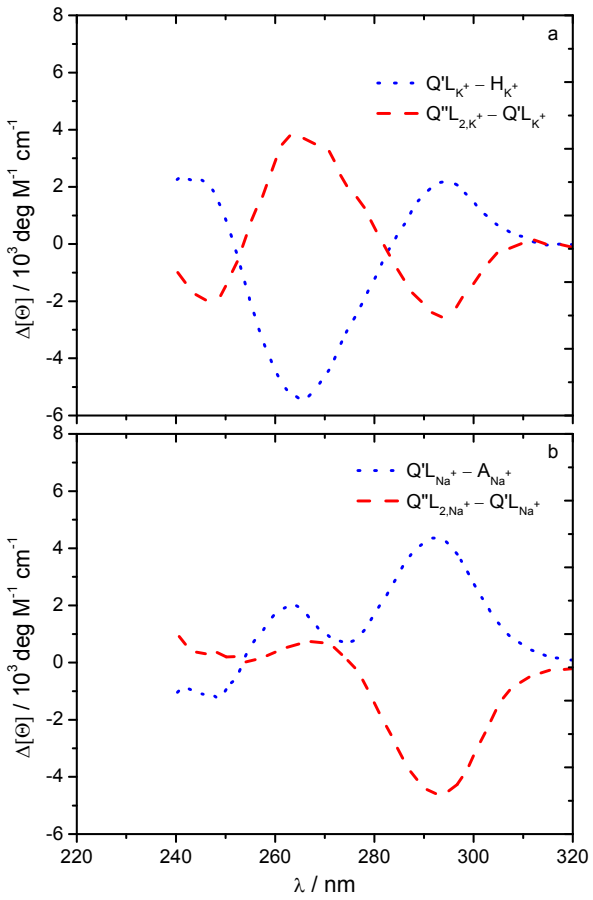

FIGURE S10 Changes of CD spectra upon ligation. Dotted lines represent differences between CD spectra of the complex with one bound ligand molecule (Phen-DC3) and ligand free quadruplex in 100 mM K^+ ($Q'L_{K}+ - H_{K}+$; panel a) and in 100 mM Na^+ ($Q'L_{Na}+ - A_{Na}+$; panel b). Dashed lines represent differences between CD spectra of the complex with two bound ligand molecules and complex with one bound ligand in 100 mM K^+ ($Q''L_{2,K}+ - Q'L_{K}+$; panel a) and in 100 mM Na^+ ($Q''L_{2,Na}+ - Q'L_{Na}+$; panel b).

Correlation between Adjustable Parameters

Representative correlation matrixes are presented in Tables S4 and S5. Correlation matrix corresponding to the global model analysis of DSC and CD data (folding/unfolding of Tel22 in presence of ions, Table S4) shows high correlation between parameters $\Delta G^{o}_{QI(T_0,X^+)}$ - Δn_{QI} (> 0.90) while in the case of global model analysis of ITC and CD data (ligand binding on Tel22, Table S5) between parameters $\Delta G^{o}_{Q''L_2(T_0,X^+)}$ - $\Delta n_{Q'L}$ and $\Delta[\Theta]_{QI}$ - $\Delta[\Theta]_{Q'L}$. Therefore, the physical meaning of these adjustable parameters may be questionable. For this reason we performed the fitting procedure starting with significantly different initial values of the adjustable parameters. The obtained best fit values of all parameters were always within the error margins presented in Table S1 and S2. Moreover, poorer agreement between the model function and experimental data was observed when highly correlated $\Delta G^{o}_{QI(T_0,X^+)}$ and Δn_{QI} or $\Delta G^{o}_{Q''L_2(T_0,X^+)}$ and $\Delta n_{Q'L}$ were varied simultaneously (at fixed best-fit values of other parameters) for the ±error($\Delta G^{o}_{QI(T_0,X^+)}$) and ±error(Δn_{QI}) or ±error($\Delta G^{o}_{Q''L_2(T_0,X^+)}$) and ±error($\Delta n_{Q'L}$) reported in Tables S1 and S2. This suggests that the parameters analyzed above are reliable within the estimated error margins (Tables S4 and S5). On the other hand, the observed high correlation between spectroscopic parameters $\Delta[\Theta]_{QI}$ and $\Delta[\Theta]_{Q'L}$ has no effect on the best-fit values of thermodynamic quantities.

TABLE S4 Correlation matrix corresponding to the global model analysis of the DSC and CD (Eqs. 3, 4) folding/unfolding data of Tel22 measured at different K^+ concentrations. Highly correlated adjustable parameters are marked red.

	$\Delta G^{o}_{QI(T_0,X^+)}$	$\Delta H^{o}_{IU(T_0)}$	Δn_{QI}	$\Delta G^{o}_{IU(T_0,X^+)}$	$\Delta H^{o}_{IU(T_0)}$	$\Delta C^{o}_{P,IU}$	Δn_{IU}	Δf_{QI}
$\Delta G^{o}_{QI(T_0,X^+)}$	1.00							
$\Delta H^{o}_{IU(T_0)}$	0.39	1.00						
Δn_{QI}	0.92	0.14	1.00					
$\Delta G^{o}_{IU(T_0,X^+)}$	0.43	-0.09	0.64	1.00				
$\Delta H^{o}_{IU(T_0)}$	0.54	-0.07	0.72	0.84	1.00			
$\Delta C^{o}_{P,IU}$	-0.61	0.04	-0.74	-0.79	-0.88	1.00		
Δn_{IU}	-0.17	-0.20	-0.04	0.40	0.10	-0.02	1.00	
Δf_{QI}	0.00	0.00	0.00	0.00	0.00	0.00	0.00	1.00

TABLE S5 Correlation matrix corresponding to the global model analysis of the ITC and CD (Eqs. 5,9) Phen-DC3 binding data on Tel22 measured at different *T* and K^+ concentrations. Highly correlated adjustable parameters are marked red.

	$\Delta G^{o}_{Q'L(T_0,X^+)}$	$\Delta H^{o}_{Q'L(T_0)}$	$\Delta G^{o}_{Q''L_2(T_0,X^+)}$	$\Delta H^{o}_{Q''L_2(T_0)}$	$\Delta C^{o}_{P,Q'L}$	$\Delta n_{Q'L}$	$\Delta[\Theta]_{QI}$	$\Delta[\Theta]_{Q'L}$	$\Delta[\Theta]_{Q''L_2}$
$\Delta G^{o}_{Q'L(T_0,X^+)}$	1.00								
$\Delta H^{o}_{Q'L(T_0)}$	-0.35	1.00							
$\Delta G^{o}_{Q''L_2(T_0,X^+)}$	0.80	0.10	1.00						
$\Delta H^{o}_{Q''L_2(T_0)}$	0.07	-0.66	-0.27	1.00					
$\Delta C^{o}_{P,Q'L}$	-0.04	0.14	0.07	0.33	1.00				
$\Delta n_{Q'L}$	0.88	-0.04	0.93	0.00	0.23	1.00			
$\Delta[\Theta]_{QI}$	0.00	0.00	0.00	0.00	0.00	0.00	1.00		
$\Delta[\Theta]_{Q'L}$	0.00	0.00	0.00	0.00	0.00	0.00	-0.94	1.00	
$\Delta[\Theta]_{Q''L_2}$	0.00	0.00	0.00	0.00	0.00	0.00	0.57	-0.78	1.00

PAGE Electrophoresis

DNA dissolved in the buffer-3%DMSO solution containing Na^+ or K^+ ions was mixed with an appropriate amount of ligand in the same buffer-3% DMSO solution to achieve 40 μM DNA solution and the desired DNA/ligand molar ratio *r*. 10 μL of these samples were mixed with 3 μL of 40 % (w/v) sucrose solution and then 10 μL of such modified sample solutions were loaded onto a 22 (w/v) polyacrylamide gel and subjected to a constant voltage of 110 V for 3.5 h. The running TBE buffer, pH = 8.2, contained 0.09 M Tris, 0.09 boric acid and 1 mM EDTA. Electrophoresis cell was placed in a water bath at 25 °C. After the electrophoresis, the gels were photographed under UV light using G-box (Syngene, Cambridge, U.K.).

PAGE mobility patterns show that ligand binding to Tel22 G-quadruplex appears to be a reversible process since the band intensity of the complex and ligand-free DNA changes with *r* ($r = c_{DNA}/c_{L,tot}$). In the case of irreversible binding process the band intensity of the complex would not be a function of *r*. The intensity of the observed mobility patterns is consistent with the calculated model-based fractions of species. PAGE does not distinguish between Q'L and Q''L_2 complexes. Mobility increases in order Q < Q'L ≈ Q''L_2 and is the same in the presence of Na^+ or K^+ ions suggesting similar structure of complexes formed in the presence of K^+ and Na^+ ions. Additional experiments were performed to test reliability of the presented PAGE results. In these experiments polyacrylamide gel itself contained 100 mM salt solution or ligand of different concentrations. The additional experiments gave results that are identical to those presented in Fig. S11.

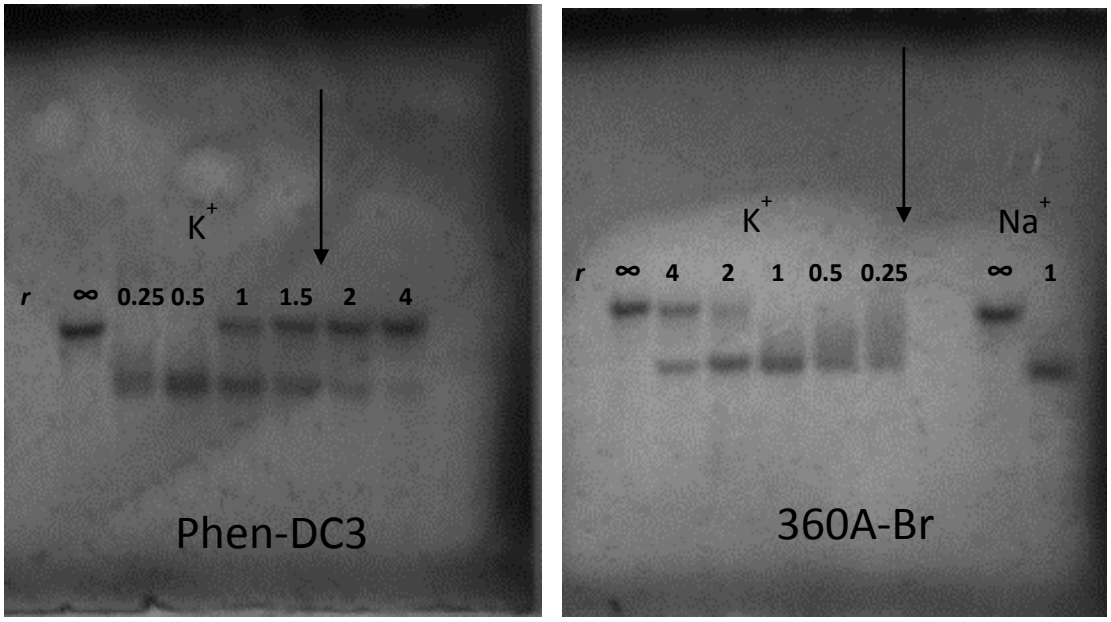

FIGURE S11 Results of PAGE electrophoresis performed at 25°C and 100 mM Na^+ or K^+. *r* is defined as DNA/ligand molar ratio.

REFERENCES

1. Bončina, M., J. Lah, I. Prislan, G. Vesnaver. 2012. Energetic basis of human telomeric DNA folding into G-quadruplex structures. *J. Am. Chem. Soc*. 134:9657-9663.
2. Luque, I., E. Freire. 2002. Structural parameterization of the binding enthalpy of small ligands. *Proteins*, 49:181-190.
3. Ciolkowski, M.L., M.M. Fang, M.E. Lund. 2002. A surface plasmon resonance method for detecting multiple modes of DNA-ligand interactions. *J. Pharm. Biomed. Anal*. 22:1037-1045.
4. Marcus, Y.A. 1986. *Ion solvation*; John Wiley & Sons Ltd.
5. Baldwin, R.L. 1986. Temperature dependence of the hydrophobic interaction in protein folding. *Proc. Natl. Acad. Sci. USA*. 83:8069-8072.
6. Finkelstein, A. V., J. Janin. 1989. The price of lost freedom - entropy of bimolecular complex-formation. *Protein Eng.* 3:1-3.